FINAL TECHNICAL REPORT

Asia Pacific Research Initiative for Sustainable Energy Systems 2021

Office of Naval Research

Grant Award Number N00014-22-1-2045

March 1, 2022 through July 15, 2025

November 12, 2025

Table of Contents

Final Technical Report
Asia Pacific Research Initiative for Sustainable Energy Systems
Grant Award Number N00014-22-1-2045
March 1, 2022 through July 15, 2025

EXECUTIVE SUMMARY

This report summarizes work conducted under Grant Award Number N00014-22-1-2045, the Asia Pacific Research Initiative for Sustainable Energy Systems 2021 (APRISES21), funded by the Office of Naval Research (ONR) to the Hawai‘i Natural Energy Institute (HNEI) of the University of Hawai‘i at Mānoa (UH). The work conducted under APRISES21 comprises research, development, testing, and evaluation (RDT&E) over a range of technical areas. These include Electrochemical Technologies with a focus on fuel cells, batteries, and electronic materials; Alternative Fuels including carbonization of biomass, marine fuels, and hydrogen; and Resilient Energy Systems including development and demonstration of advanced technologies for smart microgrids and models for reliable grid systems with a focus on resource adequacy for the Hawai‘i electrical grids. Makai Ocean Engineering, under subcontract to the University of Hawai‘i, also continued their efforts to develop high-performance, low-cost heat exchangers. A stop-work order ended this grant prior to the initial end date, which limited the completion of a portion of the work proposed and planned. A brief summary of results by major task follows.

Task 1, Program Management and Outreach, supported senior faculty and project support personnel responsible for overall program management and coordination, development and monitoring of partner and subcontract agreements, and preparation of reports and outreach materials for ONR and other stakeholders.

Task 2, Electrochemical Technologies, included RDT&E in the areas of fuel cells, Li-ion batteries, and printable electronic materials. Progress in each of these areas is summarized below.

Subtask 2.1, Fuel Cell Testing and Development, HNEI’s research comprised four projects: a) the evaluation of anion exchange membrane fuel cells; b) recovery of proton exchange membrane fuel cells exposed to SO_2 in an air stream; c) refinement of methods for electrochemical impedance spectroscopy for fuel cell evaluations; and d) contaminant removal and mitigation for fuel cell technology use in harsh environmental conditions.

2.1a) The most compelling motivation for exploring anion exchange membrane fuel cells (AEMFC) technology stems from the prospect of eliminating Pt-based catalysts from both the anode and cathode. This is due to platinum group metal (PGM)-free materials exhibiting higher

intrinsic catalytic activity towards oxygen reduction in alkaline media compared to Pt-based catalysts. PGM-free cathodes in proton exchange membrane fuel cells (PEMFC) have also exhibited tolerance to air contaminants such as CO and SO_2. Work under this award focused on establishing in-house capabilities for the fabrication of catalyst coated membranes (CCMs) and catalyst coated substrates (CCS). This was accomplished, enabling rapid screening and evaluation of novel and emerging materials that are often available only in limited quantities. Twenty-one different aspects of AEMFC manufacturing and evaluation were investigated.

2.1b) The development of simple and reliable methods to recover performance after contamination is important not only for sustaining fuel cell performance in contaminated environments, but also as a part of maintenance routines. In continuation of work under previous APRISES funding, this work evaluated potential cycling as a possible recovery method. Potential cycling was comprehensively studied using a segmented cell to assess its effectiveness and applicability to restore fuel cell performance exposed to SO_2 under different operating temperatures and currents. Results supported the feasibility and applicability of a cyclic voltammetry-induced procedure for recovering the performance of SO_2 poisoned fuel cells. The efficiency of this recovery was shown to depend on the operating cell temperature and current during the contamination. Details of this work was published in the *Journal of Power Sources* and presented at four conferences.

2.1c) HNEI continued development of advanced diagnostics. In this effort, previously developed 1d+1d impedance models of a PEMFC were extended to take into account 2D transient effects in the plane perpendicular to the channel axis, along the channel/rib coordinate. The impedance spectroscopy data obtained from HNEI's segmented cell system were used for the model fitting. The results of this work showed that resolving the impedance locally can help understand 3D local current distributions in an operating PEMFC without the need for complex 3D imaging technologies. Details of this work was published in two papers in the *Materials Research Express* journal and presented at two conferences.

2.1d) Advancement of purification technology is critical to the use of fuel cell technology into harsh environmental conditions. HNEI's previous research has shown that both SO_2 and H_2S significantly impact performance due to the irreversible binding of the contaminants. Under APRISES21 funding, detailed SO_2 gas sorption testing of the $Mg_4[OAc]_{10}[C_2mim]_2$ activated carbon composite sorbent was initiated. Testing included varying environmental conditions including humidity, flow rates, gas concentrations, relative humidity, and temperature. A preliminary comparative materials cost analysis suggests a significant cost savings with the new materials. Details of this work is currently being prepared for publication in a peer-reviewed journal.

Under Subtask 2.2, Battery Characterization and Modeling, HNEI research focused on the improvement of data-driven approaches to characterize performance and lifetime of next generation lithium-ion batteries for both DOD and commercial deployments. HNEI used *in-silico*

dataset generation in conjunction with the mechanistic battery modeling framework to test different strategies towards diagnosis and early prognosis. The emphasis of work under APRISES21 was set on realistic synthetic data covering the degradation associated with battery packs directly connected to photovoltaic systems. By using synthetic data, HNEI demonstrated possible diagnosis for days with 50% or more clear sky without the need for maintenance cycles. Results reinforced the potential of synthetic data generation and training to enable big-data studies of the behavior or deployed system that will experience sporadic usage. Details of this work was published in two papers in the *Natural Communications* and *Batteries* journals, respectively.

Under Subtask 2.3, Printable Electronic Materials, HNEI investigated transparent-conductive-flexible composites (TCFCs) as multifunctional encapsulation materials for advanced energy, aerospace, and marine applications. Two primary objectives guided the study: 1) maintain at least 50% electrical conductivity on curved surfaces relative to flat substrates and 2) preserve conductivity after 24 hours at 100°C or 100 mechanical bending cycles. Developed at HNEI's Thin Films Laboratory, these TCFCs consist of micron-sized metallic particles embedded in a transparent polymer matrix. This results in a material with high optical transmittance and low out-of-plane resistance, outperforming existing commercial transparent conductors. Their ability to function simultaneously as electrode and encapsulant—resistant to moisture and oxygen—makes them ideal for organic electronics, electrostatic dissipation, and cathodic protection. Mechanical durability was validated with both uncoated and silver-coated samples retaining conductivity. TCFCs synthesized from epoxies maintained or improved electrical performance after thermal aging at 100°C for 24 hours. These findings confirm the robustness of TCFCs under realistic environmental stresses, positioning them as next-generation encapsulants that merge barrier protection, conductivity, and optical clarity. Further customization through surface treatments offers new routes for application-specific design across photovoltaics, aerospace, defense, and soft electronics.

Under **Task 3**, Alternative Fuels, HNEI continued research in three areas: constant volume carbonization of biomass, marine fuels, and hydrogen refueling technology.

Under Subtask 3.1, Constant Volume Carbonization, HNEI investigated transient plastic phase biochars (TPPB) produced from different woody feedstocks to understand the underlying factors responsible for the differences in mechanical performance of biocarbon produced from these materials. Several analysis methods were used including proximate analysis, thermogravimetric analysis (TGA), differential scanning calorimetry (DSC), Fourier transform infrared spectroscopy (FTIR), quantitative carbon-13 nuclear magnetic resonance (^{13}C NMR), and gas chromatography-mass spectrometry (GC-MS), reactivity tests, and microscopy. Results from this study suggests that the superior mechanical performance of biocarbon produced from birch TPPB likely results from the triterpenoids acting as plasticizing agents that alter the glass transition temperature of the material. This results in more inter-particle bonding to occur during calcination increasing the

mechanical strength of the resulting biocarbon. Details of this work was submitted for publication in the *Energy & Fuels* journal and is currently under review.

Sulfur-containing compounds (SCCs) are the most abundant heteroatomic organic species (HOS) in petroleum fuels. Subtask 3.2 investigated the dynamics of SCCs in surrogate fuel systems, focusing on their oxidation stability, reactivity, and interactions. A comprehensive analysis was conducted on a selection of eleven SCCs. The investigation involved tracking the reaction and degradation processes of these SCCs at 140°C over an extended period, coupled with the analysis of resulting products to elucidate oxidation and degradation mechanisms. Interactions and reactions or binary mixtures of reactive SCCs and multicomponent SCC mixtures were examined. The study also assessed the interactions between SCCs and commercial antioxidants. Details of this work was published in the *Fuel* journal.

HNEI also continued research, development, demonstration, and assessment of hydrogen production, storage, and dispensing systems for heavy duty hydrogen vehicles, and evaluation of the operational performance of buses on the Big Island of Hawai‘i under the third subtask. Through APRISES21 funding, the team accomplished: 1) the full operational commissioning of the hydrogen station’s primary systems; 2) prepared the tube trailers for operation; 3) deployed and operated hydrogen transport trailers for fuel delivery; 4) performed repairs, upgrades, and preventative maintenance; 5) established an automated hydrogen dispensing system; and 6) demonstrated power and range increases in the buses. Various workforce training and outreach engagements were also supported as well.

Under **Task 4**, Resilient Energy Systems, HNEI continued research to enable the development of resilient, reliable, and secure energy systems operating with a high penetration of variable renewable generation technologies. The work included two closely integrated activities.

Under Subtask 4.1, Advanced Grid Technology, HNEI’s Grid System Technologies Advanced Research Team (Grid***START***) advanced the development, evaluation, and demonstration of alternative energy, distributed energy resources (DER), and enabling technologies to enhance grid reliability and resilience. Building on prior ONR-supported work, the team integrated methods such as advanced DER optimization, real-time analytics, system diagnostics, demand response, and electric vehicle (EV) and maritime electrification. Activities spanned software simulations, power hardware-in-the-loop (PHIL) testing at the Advanced Power System Laboratory (APSL), and field demonstrations on both civilian and Department of Defense (DOD) sites. Specific subtasks under APRISES21 included: a) addressing key operational and communications challenges in an advanced conservation voltage reduction (CVR) demonstration project; b) developing a holistic microgrid optimization framework for resilient and cost-effective DER and hydrogen integration; and c) demonstrating resilient DC microgrid and transportation solutions for marine environments on Coconut Island.

4.1a) HNEI, in partnership with U.S. Marine Corps Camp Butler, demonstrated the use of advanced CVR to realize energy savings on a DOD distribution feeder in Okinawa, Japan. Earlier phases developed and deployed core infrastructure, including a dedicated voltage regulator, advanced CVR control device, and supporting communications and metering systems, leading to reliable autonomous CVR operation and measurable energy savings at Camp Butler's Plaza Housing complex. Under APRISES21, the Grid***START*** team addressed challenges with reactive power dispatch by replicating and troubleshooting the field system at HNEI's APSL in Hawai‘i. This effort led to the identification and remote resolution of critical communication issues between the Volt/VAR Control (VVC) controller and photovoltaic (PV) inverters, successfully restoring full CVR operation. The project continued alternating-day CVR operations, further validating CVR effectiveness, and gathering operational data. Field testing was suspended in May due to a stop-work order, but major system milestones and technical barriers were successfully completed.

4.1b) HNEI developed and demonstrated a holistic optimization framework to design and operate resilient, cost-effective microgrids. Using the Natural Energy Laboratory of Hawai‘i Authority's (NELHA) facility on Hawai‘i Island as a real-world test case, the project created a hybrid model combining mixed-integer linear programming (MILP) with particle swarm optimization (PSO) to guide microgrid sizing, energy dispatch, and integration of DERs such as PV, batteries, and hydrogen systems. This approach enabled simulation of both everyday operations and extended outage scenarios, incorporating actual load and solar data, real-world utility rates, and NELHA's hydrogen infrastructure. The results highlighted the value of flexible DER portfolios, showing that green hydrogen and fuel cells can enhance microgrid autonomy and reliability, especially under prolonged outages, while also being financially viable over a 25-year lifespan. The project addressed practical modeling gaps by incorporating realistic hydrogen efficiency curves and provided actionable recommendations for microgrid design and operation. The framework and findings advance microgrid design for greater resilience and cost-effectiveness, with direct relevance to critical, grid-challenged regions like Hawai‘i. Details of this work was published in the *Energies* journal and in a Master of Science thesis.

4.1c) The Coconut Island DC microgrid project established a pioneering research platform on the island of Moku o Lo‘e in O‘ahu's Kāne‘ohe Bay to enhance energy security and test advanced technologies in a challenging coastal environment. Earlier phases included detailed microgrid design, installation of a 6.2 kW DC rooftop PV array, an 8 kW/8 kWh stationary battery system and commissioning of Hawai‘i's first electric pontoon research vessel (E-boat). Collaboration with international partners led to a prototype swappable battery system, later replaced with reliability with robust fixed-placement batteries in both the E-boat and a land-based EV. Under APRISES21, the team doubled solar capacity, installed 18.2 kWh batteries in the E-boat, upgraded control systems, and validated initial vehicle-to-grid (V2G) operation. System redesigns improved resilience, operational safety and energy efficiency, with DC operation yielding measurable savings for AC/LED loads. Despite the unexpected funding termination, the project solidified

Coconut Island as a model for microgrid-powered marine research, setting the stage for future advances in resilient, responsible coastal electrification and transport.

Subtask 4.2 focused on power systems analysis with a focus on resource risk assessment to ensure that the energy systems and related critical infrastructure on Oʻahu and the other Hawaiian Islands, home to the Pacific Command and the largest military bases in the Asia Pacific region, meets the reliability needs of DOD as significant amounts of variable generation technologies are integrated into the grid. This latter activity leveraged resources from the Energy Systems Development Special Fund (ESDSF) managed by HNEI (also known as "barrel tax") and supported the Memorandum of Agreement between the State of Hawaiʻi and the ASN for Energy, Installations and Environment, and also the Memorandum of Agreement between the University of Hawaiʻi (UH) and the Pacific Command.

In previous work, probabilistic analytic tools were developed to assess the reliability or island grids with very high penetration of variable renewables (solar and wind) with and without large scale energy storage. This analysis, conducted in collaboration with Telos Energy under contract to HNEI, was applied to quantify the reliability of the Oʻahu grid, pending the retirement of Oʻahu's largest generator, the AES coal plant, in September 2022. A user-friendly tool was developed to allow stakeholders to track schedule changes in replacement resources and the impact on system reliability.

Under this award, the project quantified the requirements for dispatchable firm capacity on Oʻahu and the other islands' grids as high amounts of variable renewable generation and battery storage is integrated into the grid. It was found that, even with the relatively consistent wind and solar resources such as found in Hawaiʻi, firm capacity of up to 60% of the peak load was required even when the variable renewables provided up to 90% of the total energy.

Task 5, Advanced Heat Exchanger Development, continued to support the development of high-performance thin foil heat exchangers (TFHX^{TM}) for use in seawater-refrigerant, air-water, and water-water applications. The work supported under this award was conducted between November 2024 and July 2025. In this period, Makai designed the next generation TFHX plate fabrication equipment; commissioned the new HX Testing Facility; performance tested two cassette-style 2-MWthermal TFHXs; developed concepts for large-scale seawater-water TFHXs; and prototyped new biofouling mitigation methods. Details of this work is available in Makai's report.

This final report describes the work that has been accomplished under each of these tasks, along with summaries of task efforts that are detailed in journal and other publications, including reports, conference proceedings, presentations, and patent applications. **Publications produced through these efforts are noted below and available on HNEI's website at https://www.hnei.hawaii.edu/publications/project-reports/aprises-21/.**

TASK 1: PROGRAM MANAGEMENT AND OUTREACH

As the prime recipient of the agreement from ONR, HNEI conducts research, development, testing, and evaluation across a range of alternative and enabling energy technologies, and is responsible for development and monitoring of partner and subcontract agreements. Under this task, senior HNEI staff developed and managed partner and subcontract agreements, coordinated task activities as needed, and coordinated development of outreach materials and reports for ONR and other audiences. Senior staff also engaged directly with other DOD organizations, such as the Navy Facilities Engineering Command (NAVFAC) to assess energy needs of bases in the Asia Pacific region in an effort to continue to build these partnerships, with a focus on near-term opportunities for application of emerging energy technologies into Hawai‘i bases and elsewhere in the Asia Pacific region. Details of the various partner, subcontract, and outreach activities are included in the relevant task summaries below.

TASK 2: ELECTROCHEMICAL TECHNOLOGIES

Task 2 is comprised of three subtasks that included the development and testing of fuel cells; the evaluation, characterization, and modeling of Li-ion batteries and battery systems; and the development of multi-functional novel polymers for use in photovoltaic and electrochemical systems and devices. Details of each research subtask are provided in the following sections.

2.1 Fuel Cell Testing and Development

Research under this subtask encompassed a range of activities for the development and testing of fuel cells. These projects included: a) evaluation of anion exchange membrane fuel cells; b) recovery of PEM fuel cells exposed to SO_2 in air stream; and c) further refinement of methods for electrochemical impedance spectroscopy for fuel cell evaluations. Details of the work conducted in each of these activities are described below.

2.1a Anion Exchange Membrane Fuel Cells

The most compelling motivation for exploring anion exchange membrane fuel cell (AEMFC) technology stems from the prospect of eliminating Pt-based catalysts from both the anode and cathode. This is due to the fact that platinum group metal (PGM)-free materials exhibit higher intrinsic catalytic activity towards oxygen reduction in alkaline media compared to Pt-based

catalysts. As demonstrated in previous studies, PGM-free cathodes in proton exchange membrane fuel cells (PEMFCs) exhibit tolerance to air contaminants such as CO and SO_2 [1]. This finding suggests that PGM-free AEMFCs may also possess the capacity to withstand other air impurities. AEMFCs have been shown to function effectively at elevated temperatures of approximately 100°C, a property that has been demonstrated to mitigate the adverse effects of contamination [2-3]. Finally, AEMFCs are notable for their ability to operate with liquid fuels and oxidants, a feature that enhances their versatility for a range of applications and derivative technologies.

AEMFC operation requires oxygen and water at the cathode with water produced at the anode, an arrangement that is the exact opposite of that in PEMFCs (Figure 2.1a.1). This fundamental difference makes it difficult to directly apply PEMFC membrane electrode assembly (MEA) fabrication methods to AEMFCs. Improving AEMFC performance and durability largely depends on the design of catalyst layers with optimized porosity, hydroxide ion conductivity, and thickness to ensure the formation of effective three-phase boundaries and efficient transport of reactants. The appropriate selection of gas diffusion layers (GDLs) is also essential for effective water management. Furthermore, the absence of standardized testing protocols and procedures highlights the need for tailored electrochemical diagnostics and evaluation methods specific to AEMFCs.

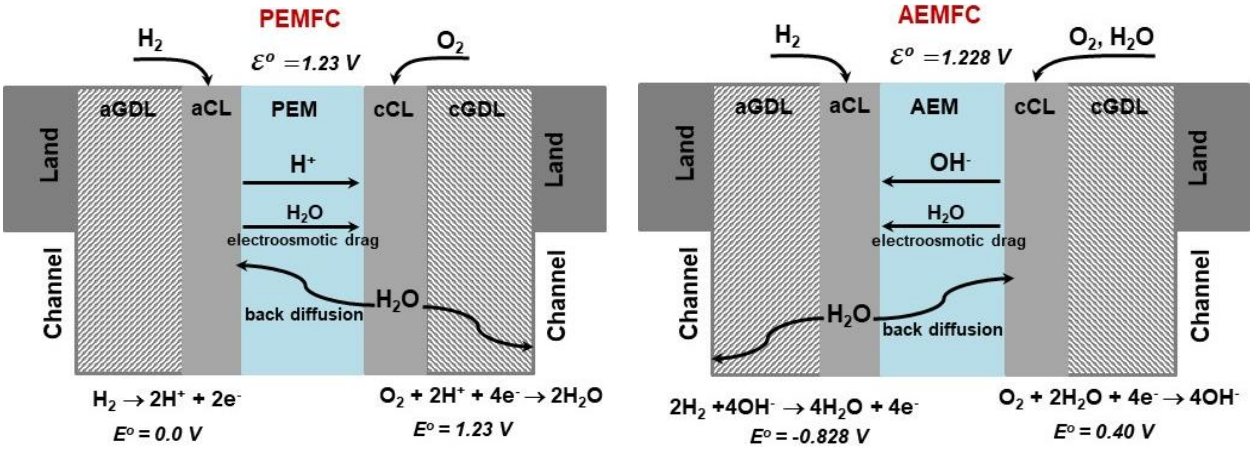

Figure 2.1a.1. Schematic representation of operation of a PEMFC (left) and an AEMFC (right).

Under this award, in-house capabilities were established for the fabrication of catalyst coated membranes (CCMs) and catalyst coated substrates (CCSs). The developed approach is readily applicable for producing CCMs and CCSs with electrode areas of 5-10 cm^2 and enables rapid screening and evaluation of novel and emerging materials, such as membranes, ionomers, and catalysts, that are often available only in limited quantities (Figure 2.1a.2).

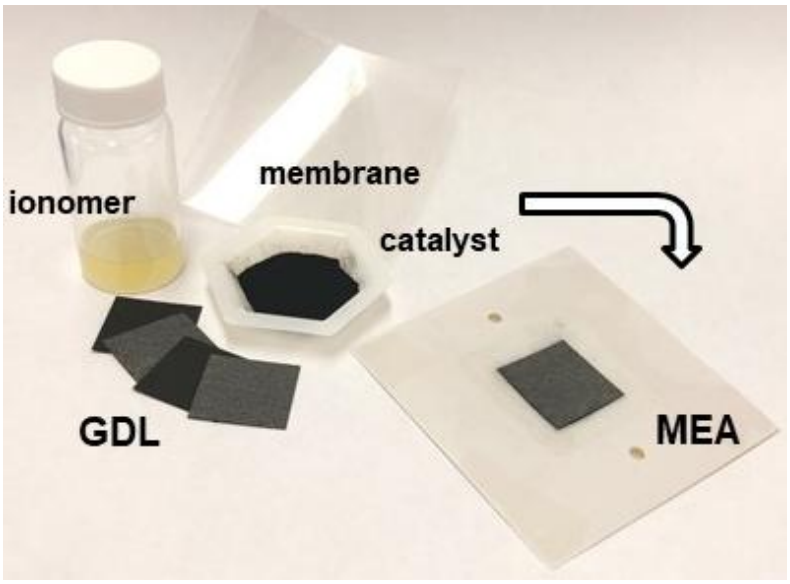

Figure 2.1a.2. Materials for AEMFC production (catalyst powder, ionomer solution, membrane, GDLs) and manufactured in-house MEA.

For understanding break-in/start-up procedure and effects of some operating conditions, we used 50% Pt/C (Vulcan XC-72) as catalyst for anode and cathode with loading of ~0.4 mg_{Pt} cm^2, while ionomer content was chosen to be 25% wt [4]. For MEAs we employed 25BC as gas diffusion layer and Teflon gaskets with 150-160 μm thickness to ensure compression of ~20-25%. Before assembling MEA, CCMs were soaked in 3 M KOH solution [4].

The AEMFC break-in procedure has been reported to be different from PEMFCs, requiring not only catalyst activation, but also water uptake and channel formation in the polymer and possibly removal of carbonate [5]. Several procedures were proposed for commercial materials [6] and it was acknowledged that variety of materials used in the AEMFC prevents establishing a standard procedure for break-in protocol. There are several possible break-in procedures for AEMFC MEAs, which can be considered: 1) potentiostatic staircase sweep from ocv to 0.1 V (100 mV step for 150 s) repeated several times [5]; 2) voltage cycling from 1 V to 0.1 V with a scan rate of 0.1 mV s^{-1}, 25 cycles [7]; 3) galvanostatic increase of current from with 200 mA cm^{-2} step [4, 8]; and 4) cell voltage hold at 0.4 V during the cell warming up [2-3].

Discussion with material manufactures (Versogen) and literature review allowed us to select break-in procedure for AEMFCs. The procedure includes constant voltage hold at 0.4 V at desired operating conditions (back, pressure, cell temperature and humidity) for several hours with monitoring HFR response until HFR reaches steady state value.

Impacts of some operation parameters on performance of AEMFCs were evaluated and it was determined effects of gas humidification on AEMFC performance and produced power density (Figure 2.1a.3). It was found that reduction in anode humidification improved the performance

since AEMFC anode is prone to flooding due to water production. The produced maximum power density was found to be 800 mW cm^{-2}.

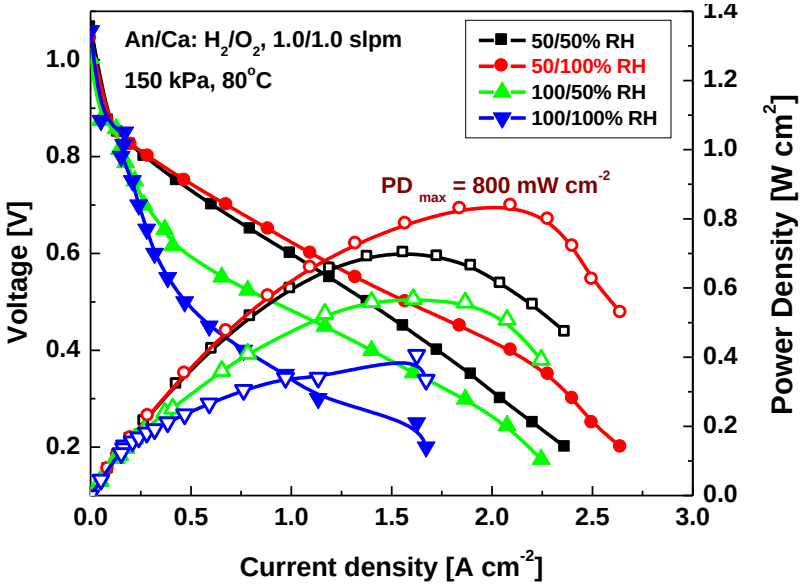

Figure 2.1a.3. IV curves and power density for AEMFCs (An/Ca: H_2/O_2, 1.0/1.0 l min^{-1}, 150 kPa, 80°C).

Studies of the in-house produced MEAs demonstrated discrepancy in performance (Figure 2.1a.4). For example, sample AEM14-20 showed better performance than others. The efforts were given to understand this observation. It was concluded that the best performing MEA was characterized by the lowest high frequency resistance and the highest electrochemical surface area (ECA) (Table 2.1a.1) which could originate through conditions of ink formulation, its preparation and deposition on the membrane. Analysis of the results suggested that impacts of temperature conditions of the catalyst ink preparation and deposition play significant role for incorporation of catalyst and ionomer in electrode structure and formation 3-phase boundaries in electrode structure. It was proposed to keep temperature of the ink manufacturing, ultrasound treatment at 10-15°C for 1 hour, while deposition of the ink on membrane at 70-80°C.

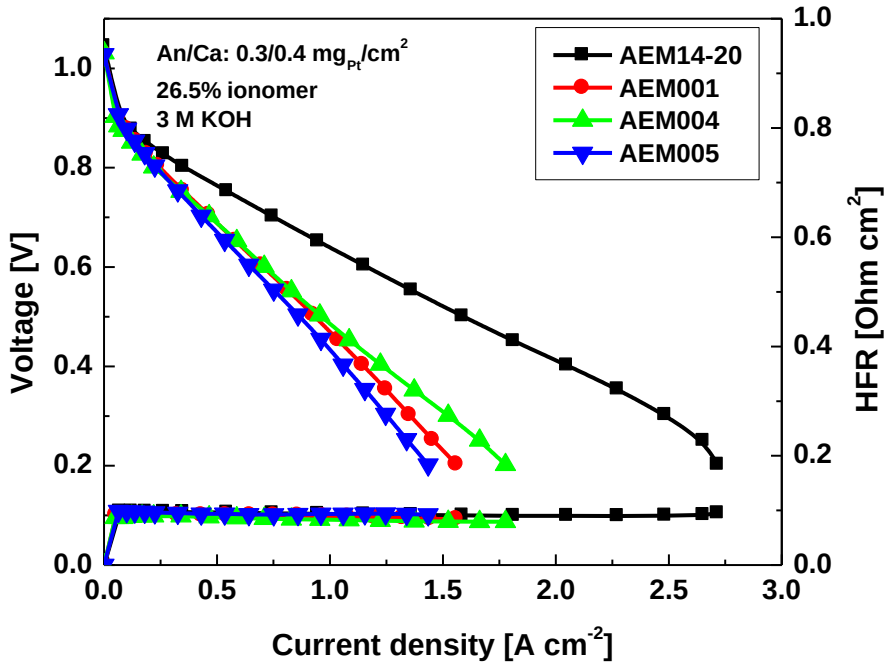

Figure 2.1a.4. IV curves and HFR values for the MEAs demonstrating nonconsistency in performance (An/Ca: H_2/O_2, 1.0/1.0 l min^{-1}, 100/100% RH, 150 kPa, 80°C).

Table 2.1a.1. Main electrochemical parameters for the sample from Figure 2.1a.4: Electrochemical surface area (ECA) for anode and cathode, HFR values and ionic resistivity (R_{ion}).

Sample	ECA_{ca} [$m^2 g^{-1}$]	ECA_{ca} [$m^2 g^{-1}$]	HFR [Ohm cm^2]	R_{ion} [Ohm cm^2]
AEM14-20	12.19	3.65	0.0397	0.368
AEM001	5.28	5.75	0.0694	0.341
AEM004	9.9	1.25	0.0546	0.161
AEM005	9.58	6.24	0.0566	0.276

The other aspect of AEMFCs operation is chemistry of ionomer and membrane. AEM head groups have traditionally been quaternary ammonium (QA) ions. QA ions are positively-charged polyatomic ions of the structure $[NR_4]^+$, where R is any organic group. Unlike the (NH^+_4) and the primary, secondary, or tertiary ammonium cations, the QA are permanently charged, independent of the pH of their solution. QA ions are synthesized by quaternization process when polymer containing amine groups reacts with alkyl halide (e.g. chlorine, bromide, iodide).

The quaternized materials must go through alkalization treatment in KOH to exchange Hal^- to OH^-. Moreover, anion exchange membranes are available in HCO_3^- form and need to be transformed to OH^-. To achieve this treatment 3 strategies were evaluated: 1) CCM long-term soaking in 4 M KCl for 96 hours and an additional 3 hours in 3 M KOH; 2) long-term (48 hours) soaking of the catalyst coated membrane (CCM) in 3 M KOH; and 3) short-term soaking of the CCM in 3 M KOH (3 hours). Figure 2.1a.5 presents the results of the pretreatment evaluation. It was found that the long-term soaking via #1 and #2 strategies did not show significant benefits compared to

short-term soaking in KOH (#3). So, pretreatment #3 was chosen for the simplicity and time saving of the MEA preparation.

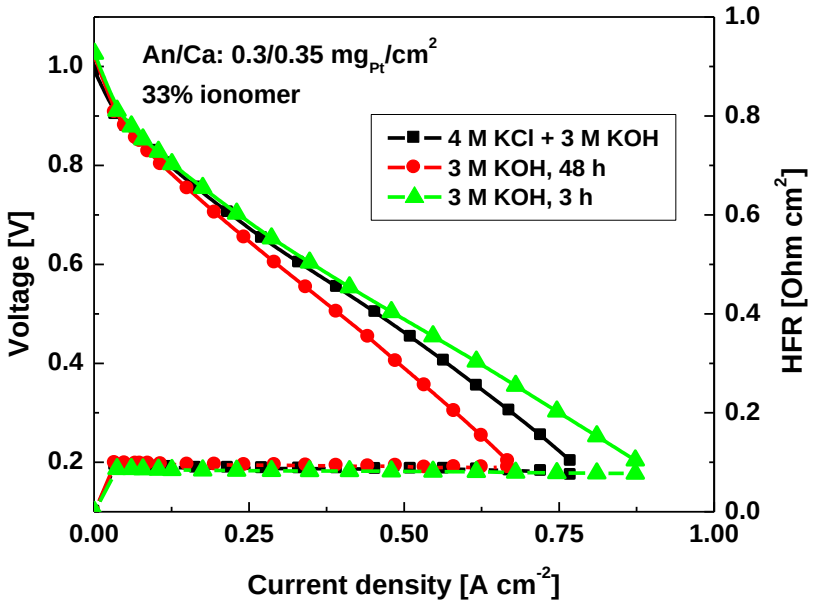

Figure 2.1a.5. IV curves and HFR values for the MEAs demonstrating effect of KOH pretreatment (An/Ca: H_2/O_2, 1.0/1.0 l min^{-1}, 100/100% RH, 150 kPa, 80°C).

The application of PtRu/C dual-function bimetallic hydrogen oxidation electrocatalyst brings several advantages to AEMFC such as reducing adsorption energy of QA groups compared to Pt and improves hydrogen oxidation reaction (HOR) in alkaline media [9]. Figure 2.1a.6 clearly indicate that PtRu/C anode containing fuel cell demonstrated higher performance than pure Pt/C sample. Cyclic voltammetry (CV) scans demonstrate typical Pt and PtRu features (Figure 2.1a.7).

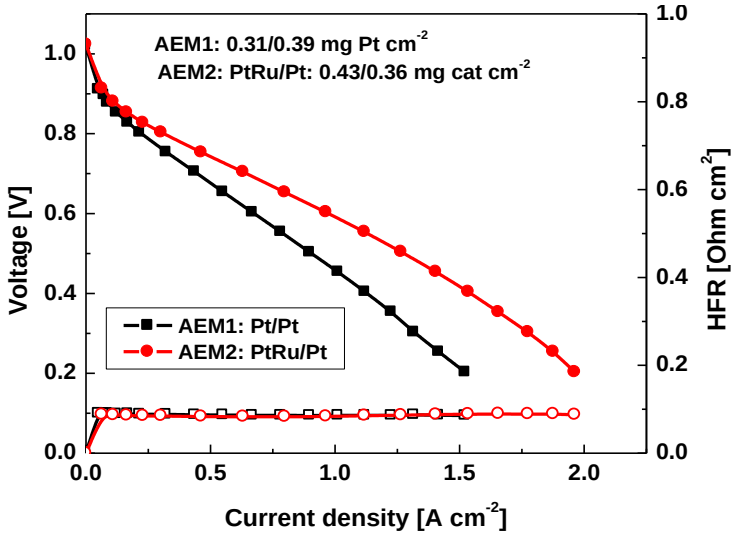

Figure 2.1a.6. IV curves and HFR values for the MEAs demonstrating effect of anode catalyst: Pt vs PtRu. An/Ca: H_2/O_2, 1.0/1.0 l min^{-1}, 100/100% RH, 150 kPa, 80°C.

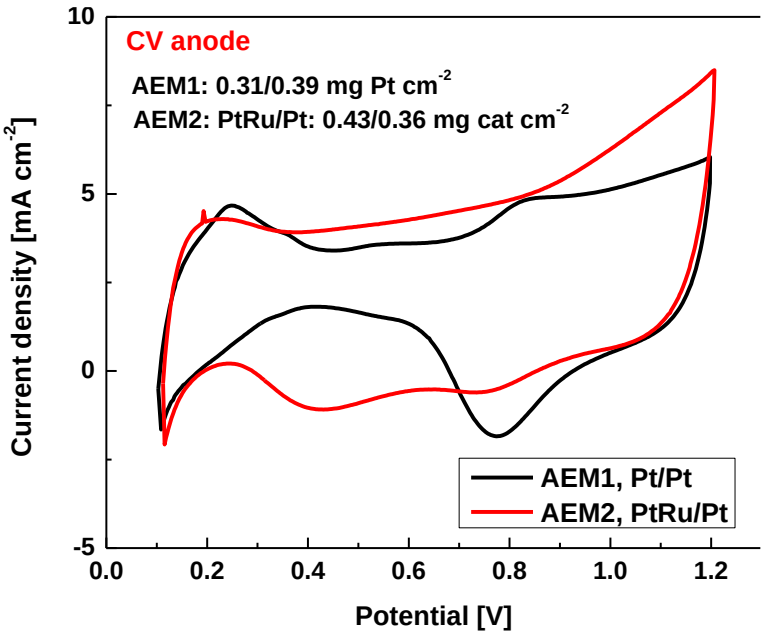

Figure 2.1a.7. CV scans of MEAs employing Pt/C and PtRu/C catalysts for anode (An/Ca: N_2/H_2, 0.5/0.5 l min^{-1}, 100/100% RH, 150 kPa, 80°C).

Under this award's funding, twenty-one different aspects of AEMFC manufacturing and evaluation were investigated. The following key achievements were accomplished:

1. In-house capabilities for manufacturing catalyst-coated membranes and catalyst-coated substrates were established, enabling rapid screening and evaluation of new materials;
2. Break-in procedures for AEMFCs were optimized, recognizing their differences from PEMFCs. Based on literature review and discussions with manufacturers, holding the cell voltage at 0.4 V under operating conditions was selected as the most effective approach;
3. Operational parameters, particularly gas humidification, were shown to significantly impact AEMFC performance. Reduced anode humidification improved power density, achieving values up to 800 mW cm^{-2};
4. Compression ratio studies identified an optimal range of 20-25% to ensure MEA durability and stable performance;
5. Variability in MEA performance was observed, with higher ECA and lower high-frequency resistance (HFR) correlating with better results. Ink preparation temperature and deposition conditions were identified as critical factors influencing catalyst layer quality;
6. Pretreatment of CCMs in KOH was necessary for ionomer alkalization. A short-term KOH soak (3 hours) was found to be as effective as longer treatments, simplifying MEA preparation; and
7. The application of PtRu/C bimetallic catalysts improved hydrogen oxidation reaction activity and overall fuel cell performance compared to conventional Pt/C catalysts.

References

[1] Reshetenko, T., Serov, A., Artyushkova, K., Matanovic, I., Sarah Stariha, & Atanassov, P. (2016). Tolerance of non-platinum group metals cathodes proton exchange membrane fuel cells to air contaminants. *Journal of Power Sources*, *324*, 556–571. https://doi.org/10.1016/j.jpowsour.2016.05.090

[2] Douglin, J. C., Varcoe, J. R., & Dekel, D. R. (2020). A high-temperature anion-exchange membrane fuel cell. *Journal of Power Sources Advances*, *5*, 100023. https://doi.org/10.1016/j.powera.2020.100023

[3] Douglin, J. C., Singh, R. K., Haj-Bsoul, S., Li, S., Biemolt, J., Yan, N., Varcoe, J. R., Rothenberg, G., & Dekel, D. R. (2021). A high-temperature anion-exchange membrane fuel cell with a critical raw material-free cathode. *Chemical Engineering Journal Advances*, *8*, 100153. https://doi.org/10.1016/j.ceja.2021.100153

[4] Wang, T., Shi, L., Wang, J., Zhao, Y., Setzler, B. P., Rojas-Carbonell, S., & Yan, Y. (2019). High-performance hydroxide exchange membrane fuel cells through optimization of relative humidity, backpressure and catalyst selection. *Journal of The Electrochemical Society*, *166*(7). https://doi.org/10.1149/2.0361907jes

[5] Novalin, T., Pan, D., Lindbergh, G., Lagergren, C., Jannasch, P., & Lindström, R. W. (2021). Electrochemical performance of poly(arylene piperidinium) membranes and ionomers in anion exchange membrane fuel cells. *Journal of Power Sources*, *507*, 230287. https://doi.org/10.1016/j.jpowsour.2021.230287

[6] Mustain, W. E., Chatenet, M., Page, M., & Kim, Y. S. (2020). Durability challenges of anion exchange membrane fuel cells. *Energy & Environmental Science*, *13*(9), 2805–2838. https://doi.org/10.1039/d0ee01133a

[7] Carlson, A., Shapturenka, P., Eriksson, B., Lindbergh, G., Lagergren, C., & Wreland Lindström, R. (2018). Electrode parameters and operating conditions influencing the performance of anion exchange membrane fuel cells. *Electrochimica Acta*, *277*, 151–160. https://doi.org/10.1016/j.electacta.2018.04.137

[8] Weiss, C. M., Setzler, B. P., & Yan, Y. (2022). Study of cathode gas diffusion architecture for improved oxygen transport in hydroxide exchange membrane fuel cells. *Journal of The Electrochemical Society*, *169*(5), 054505. https://doi.org/10.1149/1945-7111/ac6446

[9] Matanovic, I., & Kim, Y. S. (2023). Electrochemical phenyl oxidation: A limiting factor of oxygen evolution reaction in water electrolysis. *Current Opinion in Electrochemistry*, *38*, 101218. https://doi.org/10.1016/j.coelec.2023.101218

2.1b Recovery of PEM Fuel Cells Exposed to SO_2 in an Air Stream

The application of proton exchange membrane fuel cells (PEMFC) requires enhanced durability for operation in various environments. The operation of PEMFCs using ambient air has demonstrated the negative impacts of common air impurities like SO_2, NO_2, and volatile organic compounds. Performance drop originating from exposure to majority of the airborne contaminants can be self-recovered by operating the fuel cell with pure air. However, SO_2 causes irreversible

performance loss due to the electrochemical reduction of S-containing species adsorbed on Pt and the formation of elemental sulfur [1].

In practice, the implementation of air filtration systems in PEMFCs is required to prevent loss of performance, but the application of air filters and adsorbents is limited by pollutant bypass, material attrition, or saturation. Therefore, the development of simple and reliable recovery methods is important not only for sustaining fuel cell performance in contaminated environments but also as a part of maintenance routines. Understanding the mechanism of SO_2 contamination of the fuel cell cathode due to S^0 deposition of Pt suggests a possible recovery approach that includes an increase in cathode potential to values where S^0 can be electro-oxidized to soluble products and removed from the electrode. Currently, several methods have been shown to recover PEMFC performance after cathode exposure to SO_2: 1) cathode purge by pure air at flow rates of 10 l min^{-1} [2]; 2) potential cycling [3**Error! Bookmark not defined.**]; 3) multiple measurements of polarization curves [3]; and 4) injection of ~0.4% O_3 in an air stream for 15 minutes [4]. These published results show that the proposed recovery strategies were successful for chosen conditions, but to the best of our knowledge, there were no studies on the limitations of these methods. Moreover, implementation of these recovery approaches in practical applications might be restricted or even impossible by the overall PEMFC system, which includes not only fuel cell stacks but also H_2/air pumps, compressors, humidifies, batteries, and electronics.

In this work, a potential cycling as recovery procedure was comprehensively studied to assess its effectiveness and applicability to restore fuel cell performance exposed to SO_2 under different conditions such as operating temperature and current using segmented cell approach.

The experimental work was performed using a segmented cell test system developed at HNEI [5]. Commercially available 100 cm^2 catalyst coated membranes with Pt content of 0.1 and 0.4 mg_{Pt} cm^{-2} for both anode and cathode, respectively, were used in this work. SO_2 concentration in air stream was 5 ppm. The poisoning proceeded until the cell voltage reached a steady state; after that, SO_2 injection was stopped to assess the self-recovery in pure air, followed by the recovery procedure which consisted of cyclic voltammetry (CV) from 0.1 to 1.2 V for 10 cycles at 20 mV/s. The MEA was operated at stoichiometry of 2 for anode and cathode, 150 kPa back pressure. Cell temperature was 60 and 80°C, and the overall current density was 0.6 and 1.0 A cm^{-2}.

The PEMFC performance under SO_2 exposure was studied under galvanostatic control with cell current densities of 0.6 and 1.0 A cm^{-2} and cell temperatures of 60 and 80°C. The localized PEM fuel cell behavior under various operating conditions is shown in Figures 2.1b.1 and 2.1b.2 in terms of the segment voltage and normalized individual segment current profiles. Normalized current density was defined as a ratio between a measured current density and its initial value determined during the pre-poisoning step when the samples were operated with pure air within the first 14-15 hours to estimate the baseline performance. Table 2.1b.1 provides a summary of the performance of the MEAs during the poisoning and recovery experiments. Results demonstrated

that at the chosen flow field design, an increase in the operating temperature did not improve the initial performance. The cell voltage at the pre-poisoning stage was 0.735 V and 0.730 V at 0.6 A cm^{-2} for 60 and 80°C, respectively. At 1.0 A cm^{-2}, the initial cell potential was found to be 0.680 and 0.670 V for 60 and 80°C, respectively.

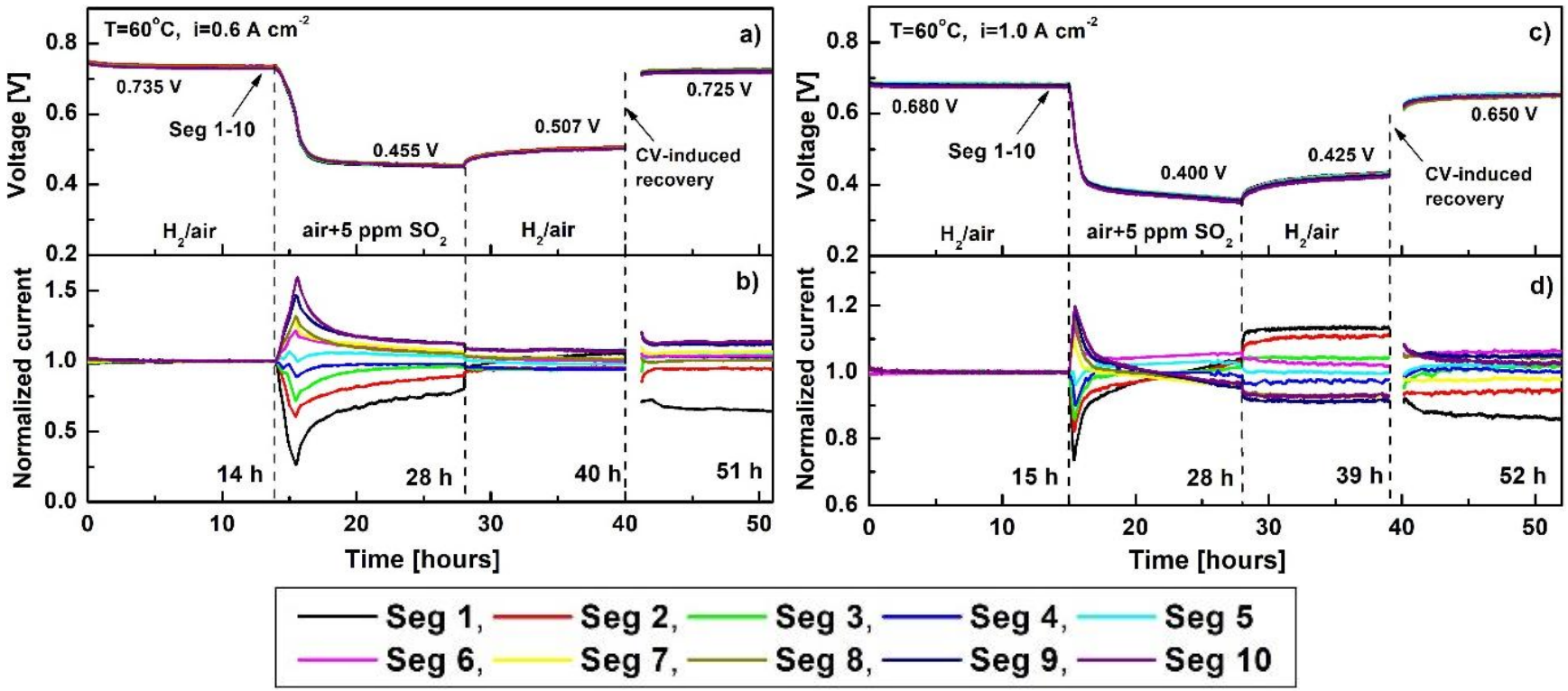

Figure 2.1b.1. Voltage and normalized current density profiles of individual segments under 5 ppm SO_2 cathode exposure, self-recovery and CV-induced recovery: (a, b) 0.6 A cm^{-2}, (c, d) 1.0 A cm^{-2} (Anode/cathode: H_2/air, 2/2 stoichiometry, 100/50% RH, 150/150 kPa, 60°C).

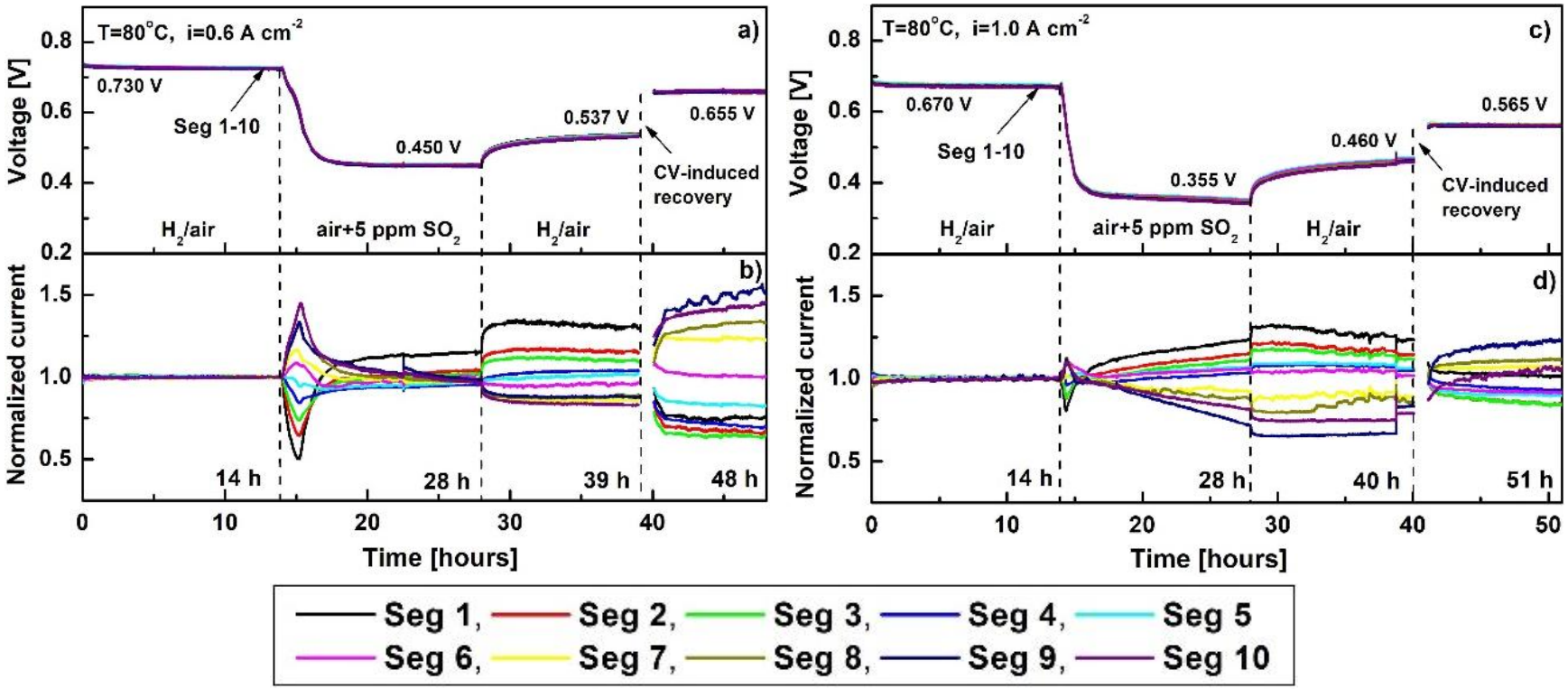

Figure 2.1b.2. Voltage and normalized current density profiles of individual segments under 5 ppm SO_2 cathode exposure, self-recovery and CV-induced recovery: (a, b) 0.6 A cm^{-2}, (c, d) 1.0 A cm^{-2} (Anode/cathode: H_2/air, 2/2 stoichiometry, 100/50% RH, 150/150 kPa, 80°C).

Table 2.1b.1. Initial cell voltage of the samples (V_0) during exposure to 5 ppm SO_2 (V_{SO2}), self-recovery ($V_{self\text{-}rec}$), after the CV-induced recovery (V_{CV}), performance drop (ΔV), and recovery as a ratio between V_{CV} and V_0.

Sample	i [A cm^{-2}]	T [°C]	V_0 [V]	V_{SO2} [V]	$V_{self\text{-}rec}$ [V]	V_{CV} [V]	ΔV [mV]	Recovery [%]
MEA-0.6-60	0.6	60	0.735	0.455	0.507	0.725	10	99
MEA-1.0-60	1.0	60	0.680	0.400	0.425	0.650	30	95
MEA-0.6-80	0.6	80	0.730	0.450	0.537	0.660	75	90
MEA-1.0-80	1.0	80	0.670	0.355	0.460	0.562	105	84

The introduction of 5 ppm SO_2 in the air stream led to a rapid drop in the segment voltage with an inflection point at ~0.62-0.63 V for 0.6 A cm^{-2} and 0.55-0.56 V at 1.0 A cm^{-2}. At steady state conditions after several hours of SO_2 contamination, the performance decreased by 280 mV for both current densities at 60°C; while at 80°C, the cell voltage drop was 280 mV at 0.6 A cm^{-2} and 315 mV at 1.0 A cm^{-2}. At the same time, a redistribution of local current revealed similar patterns for all samples and studied operating conditions. At the beginning of the contamination, the current densities of inlet segments 1-5 decreased, while outlet segments 6-10 produced higher currents. The segment currents reached their maximum values at the potential of the inflection point in the voltage profiles (0.55-0.63 V), and a reversal of the local performance was detected in which the generated current increased for segments 1-5 and deceased for segments 6-10. The inflection points at the voltage profiles and simultaneous drastic current redistribution together with electrochemical impedance spectroscopy results showing low-frequency inductance indicated on electro-reduction of SO_x, occurring in parallel with oxygen reduction reaction (ORR). The similar behavior pattern was previously observed in our works for PEMFCs exposed to C_2H_2, CH_3CN, CH_3Br, and naphthalene which also went through electro-reduction together with ORR.

After passing the inflection point and going through electro-reduction of SO_2, the current distribution appeared to depend on kinetics of local Pt coverages by various S-containing species, oxygen, and water. The current distribution pattern proposed that after SO_x electro-reduction, there was a partial electrochemical surface area (ECA) recovery of the segment 1-4 and redistribution of the S-containing species downstream. It should be noted that the reduced products remained on the Pt surface, competed, and suppressed ORR and SO_2 adsorption from the gas phase. A comparison of 0.6 and 1.0 A cm^{-2} data sets showed: 1) a transition time for the fuel cell to reach a steady state was shorter for high current operation and 2) a potential of the inflection point was lower for high current. The observations could be attributed to different initial cell potential and different water production rate within MEAs.

The operation of the MEAs in pure air immediately after cathode poisoning resulted in partial recovery of the performance and further local current distribution. The lack of full recovery could be explained by the fact that, during the self-recovery stage, it is possible that only weakly bonded SO_x species were removed from Pt, while formed S^0 and strongly adsorbed other S-containing species still covered the electrocatalyst surface [1, 6, 7]. To recover the ECA, it is necessary to increase the cell potential to values where S^0 can be oxidized. Therefore, to evaluate this approach, we applied the CV-induced recovery procedure. The cycling was performed in the potential range of 0.1 to 1.2 V [3]. The obtained results clearly showed that CV can further recover the cell voltage under certain conditions (operating current and cell temperature) and almost restored initial performance. The CV-induced recovery of the MEA contaminated at 0.6 A cm^{-2} and 60°C led to cell potentials of 0.725 V vs. an initial performance of 0.735 V, which corresponded to 99% recovery and indicated full recovery (Figures 2.1b.1a and 2.1b.1b). At the same time, operation at higher temperature and lower cell potential (or higher operating current) resulted in more

pronounced differences between the initial and recovered performances, such as 105 mV for 1.0 A cm^{-2} and 80°C (84% of recovery) (Figures 2.1b.2c and 2.1b.2d).

Figure 2.1b.3a presents IV curves collected for the total cells before (BOT) and after (EOT) SO_2 exposure and recovery. It should also be mentioned that polarization curves were measured after the CV procedure used for the ECA determination. The obtained results demonstrated that the performance drop at a temperature of 60°C was 10 and 40 mV after cathode contamination at 0.6 and 1.0 A cm^{-2}, respectively (Figures 2.1b.3a and 2.1b.3b). These observed voltage drops were found to be similar to the cell performance immediately after CV-induced recovery (Figures 2.1b.1a and 2.1b.1c and Table 2.1b.1). An increase in the operating temperature to 80°C caused cell voltage declines of 30 and 60 mV recorded at 1.0 A cm^{-2} for low- and high-current SO_2 poisoning, respectively (Figures 2.1b.3c and 2.1b.3d). These values of the cell voltage were higher than the performance detected after CV-induced recovery (Figures 2.1b.2a and 2.1b.2b and Table 2.1b.1). Apparently, CV-induced recovery could not restore cell performance at 80°C, and the additional CV procedure may contribute to further recovery of the voltage. A comparison of the curves shows that performance behavior caused by SO_2 contamination and subsequent recovery depended on operating conditions such as cell temperature and current density.

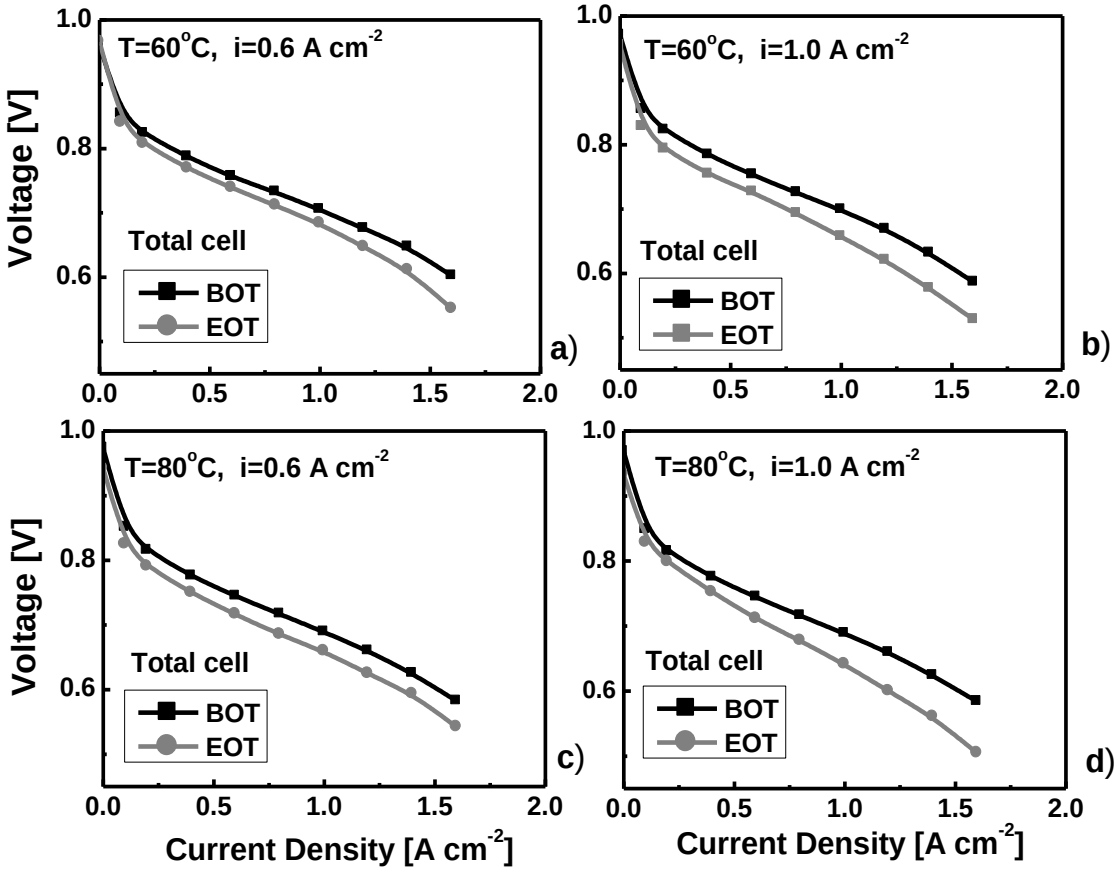

Figure 2.1b.3. BOT and EOT polarization curves for the total cell after 5 ppm SO2 exposure at a) 60°C and i = 0.6 A cm-2, b) 60°C and 1.0 A cm-2, c) 80°C and 0.6 A cm-2, and d) 80°C and 1.0 A cm-2 (An/Ca: H2/air, 2/2 stoichiometry, 100/50% RH, 150/150 kPa).

It was found that the anode and cathode ECA losses were 3-5 and 8-11%, respectively, for 60°C, while an increase in the cell temperature to 80°C caused ECA drops of 15 and 22-23% for the anode and cathode, respectively.

The obtained data clearly present the feasibility and applicability of the CV-induced procedure for recovering the performance of SO_2 poisoned fuel cells. The efficiency of this recovery was shown to depend on the operating cell temperature and current during the contamination.

More detail on this work can be found in the *Journal of Power Sources* publication listed below.

Publications and Presentations

Peer-Reviewed Publications

1. Reshetenko, T. V. (2023). Impacts of operating conditions on the recovery of proton exchange membrane fuel cells exposed to sulfur dioxide in an Air Stream. *Journal of Power Sources, 559*, 232676. https://doi.org/10.1016/j.jpowsour.2023.232676

Conference Proceedings and Presentations

1. Reshetenko, T. (2024, October 6-11). *Comprehensive evaluation of PEM fuel cells recovery exposed to sulfur dioxide in air stream, I01A-2643*. 246th Electrochemical Society Meeting, Honolulu, HI, USA.
2. Reshetenko, T., Ben, B. L., Laue, V., Krewer, U., Artyushkova, K. (2023, February 7-9). *PEM fuel cells performance in real-world environmental conditions*. Hydrogen and Fuel Cell Seminar, Long Beach, CA, USA.
3. Reshetenko, T., Ben, B. L., Laue, V., Krewer, U., Artyushkova, K. (2022, September 5-7). *Operation of PEM fuel cells exposed to harsh environments*. GDE Symposium, Mardeburg, Germany.
4. Reshetenko, T., Ben, B. L., Laue, V., Krewer, U., Artyushkova, K. (2021, December 16-21). *Spatial low-Pt PEMFCs performance and durability under cathode exposure to common air contaminants*. International Chemical Congress of Pacific Basin Societies (Pacifichem), Honolulu, HI, USA.

References

[1] Hyun, J., & Kim, H.-T. (2023). Powering the hydrogen future: Current status and challenges of anion exchange membrane fuel cells. *Energy & Environmental Science*, *16*(12), 5633–5662. https://doi.org/10.1039/d3ee01768k

[2] Baturina, O. A., Gould, B. D., Korovina, A., Garsany, Y., Stroman, R., & Northrup, P. A. (2011). Products of SO_2 adsorption on fuel cell electrocatalysts by combination of Sulfur K-Edge Xanes and Electrochemistry. *Langmuir*, *27*(24), 14930–14939. https://doi.org/10.1021/la2033466

[3] Jayaraj, P., Karthika, P., Rajalakshmi, N., & Dhathathreyan, K. S. (2014). Mitigation studies of sulfur contaminated electrodes for PEMFC. *International Journal of Hydrogen Energy*, *39*(23), 12045–12051. https://doi.org/10.1016/j.ijhydene.2014.06.011

[4] Gould, B. D., Bender, G., Bethune, K., Dorn, S., Baturina, O. A., Rocheleau, R., & Swider-Lyons, K. E. (2010). Operational performance recovery of so[sub 2]-contaminated proton exchange membrane fuel cells. *Journal of The Electrochemical Society*, *157*(11). https://doi.org/10.1149/1.3483108

[5] Kakati, B. K., Unnikrishnan, A., Rajalakshmi, N., Jafri, R. I., Dhathathreyan, K. S., & Kucernak, A. R. J. (2016). Recovery of polymer electrolyte fuel cell exposed to sulphur dioxide. *International Journal of Hydrogen Energy*, *41*(12), 5598–5604. https://doi.org/10.1016/j.ijhydene.2016.01.077

[6] Reshetenko, T., Laue, V., Krewer, U., & Artyushkova, K. (2019). Poisoning effects of sulfur dioxide in an air stream on spatial proton exchange membrane fuel cell performance. *Journal of Power Sources*, *438*, 226949. https://doi.org/10.1016/j.jpowsour.2019.226949

[7] Reshetenko, T., Laue, V., Krewer, U., & Artyushkova, K. (2020). Study of degradation and spatial performance of low PT-loaded proton exchange membrane fuel cells under exposure to sulfur dioxide in an oxidant stream. *Journal of Power Sources*, *458*, 228032. https://doi.org/10.1016/j.jpowsour.2020.228032

2.1c Electrochemical Impedance Spectroscopy for Fuel Cell Evaluation

It is well known that water management is an important issue for PEM fuel cell performance. In particular, oxygen transport through the porous gas-diffusion layer (GDL) depends on the GDL water content. Large amount of liquid water produced in the ORR could flood the GDL blocking the oxygen transport to adjacent domain of the catalyst layer. In the past two decades, significant work has been done to visualize liquid water distribution and dynamics in an operating PEM fuel cell. In operando water imaging is typically done using either X-ray tomography or neutron radiography. However, both techniques require unique and expensive equipment (synchrotron radiation or neutron beam source).

In the context of present work, particular interest is in the distribution of liquid water under the channel and rib (land) GDL areas. Muirhead *et al*. [1] reported X-ray tomography of water distribution in the plane perpendicular to the air channel in the cell equipped with the Sigracet 25 BC GDL. 25BC is the carbon paper formed by straight in-plane carbon fibers fixed by PTFE; the paper is coated with MPL. It was demonstrated that strong non-uniformity of water distribution with high water content under the land (rib) and low water content under the channel.

In this work, we extend our previous 1d+1d impedance model of a PEMFC to take into account 2D transient effects in the plane perpendicular to the channel axis, along the channel/rib coordinate. The oxygen diffusion coefficient in the GDL is allowed to vary along the y-coordinate which seems to be reasonable given the strong non-uniformity of water content.

The impedance spectroscopy data obtained by HNEI's segmented cell system were used for the model fitting. It should be noted that 2D distributions of the oxygen concentration C_b (x, y) in the segments 1 (air inlet), 5 (middle), and 9 (close to the outlet) together with the distributions of local current density along the y-coordinate are shown in Figure 2.1c.1for the mean cell current density of 800 mA cm^{-2}. As can be seen, quite large gradients of the oxygen concentration lead to a strong non-uniformity of the local current density. At the mean current density of about 800 mA cm^{-2}, local current under the channel is close to 1100 mA cm^{-2}; while under the rib, it drops down to 400 mA cm^{-2} (Figure 2.1c.1). However, at lower current density (200 mA cm^{-2}), the oxygen concentration and local current are practically uniform under the channel and rib (Figure 2.1c.2).

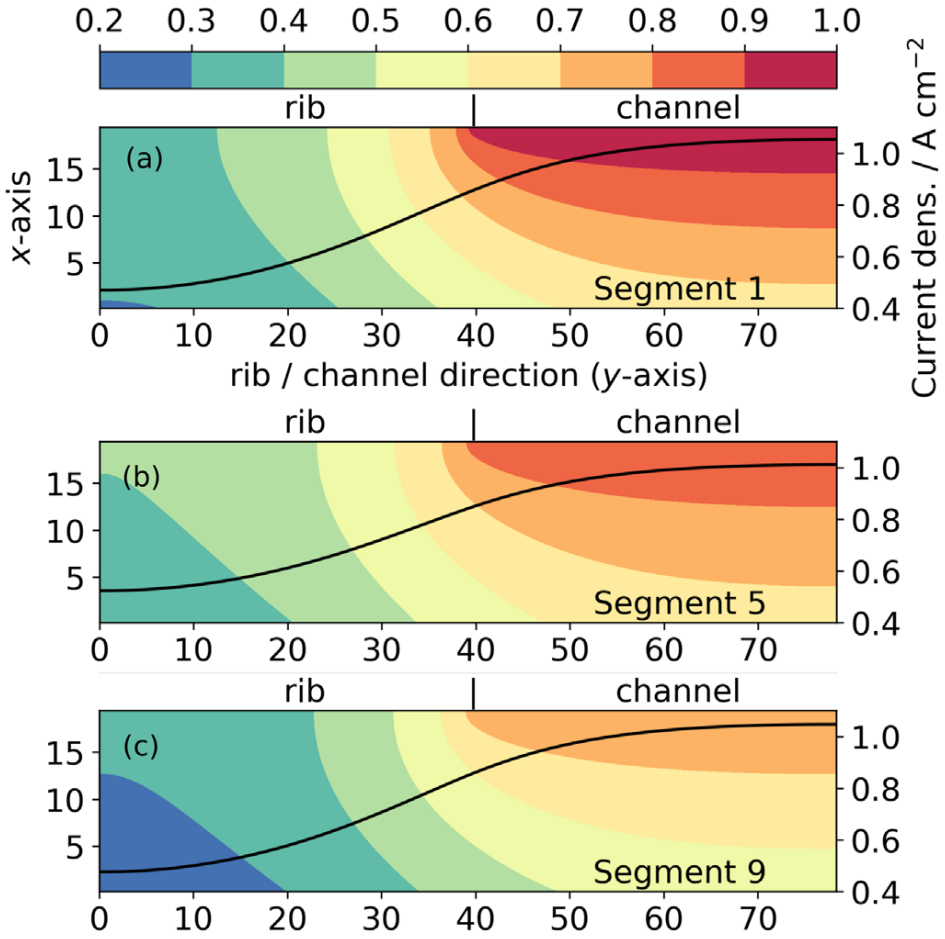

Figure 2.1c.1. 2D distribution of the scaled oxygen concentration under the rib and channel in segments a) 1, b) 5, and c) 9 (Solid lines: local current density along the rib/channel coordinate y. Mean current density in the cell is 800 mA cm^{-2}).

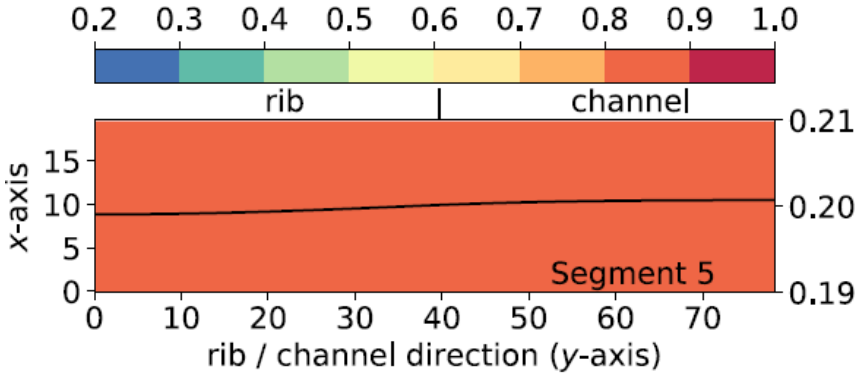

Figure 2.1c.2. 2D distribution of the scaled oxygen concentration under the rib and channel in segment 5 (Mean current density in the segment is about 200 mA cm^{-2}. Solid line: local current density along the rib/channel coordinate y).

Fitting of the model to measure impedance spectra of a segmented PEMFC equipped with the Sigracet 25BC GDL gave the following results:

1. The contribution of oxygen transport under the rib to the cell impedance is marginal, which does not allow to reliably determine the oxygen diffusivity of the GDL domain under the rib. Possible local water accumulation under the ribs hence does not affect the effective oxygen transport properties of Sigracet 25BC;
2. The effective oxygen diffusivity of Sigracet 25BC GDL is about 0.02-0.03 $cm^2\ s^{-1}$;
3. At the current density of 800 mA cm^{-2}, oxygen concentration is strongly non-uniform with this concentration under the channel being nearly three times higher than under the rib. Low oxygen concentration is due to large oxygen transport distance under the rib;
4. At the current density of 800 mA cm^{-2}, local current density is also strongly non-uniform with almost three times higher value under the channel than under the rib; and
5. However, at lower cell current density (200 mA cm^{-2}) both the oxygen concentration and local current are fairly uniform between the channel and rib.

To summarize, the results show that local EIS is a useful tool for studying 3D local current distribution in an operating PEM fuel cell.

More detail on this work can be found in the *Materials Research Express* publications listed below.

Publications and Presentations

Peer-Reviewed Publications

1. Reshetenko, T., & Kulikovsky, A. (2023). Oxygen transport in the low–PT catalyst layer of a PEM fuel cell: Impedance spectroscopy study. *Materials Research Express*, *10*(1), 015501. https://doi.org/10.1088/2053-1591/acaef3
2. Reshetenko, T., & Kulikovsky, A. (2023). A quasi three–dimensional model for PEM fuel cell impedance: The effect of local oxygen depletion under the flow field rib. *Materials Research Express*, *10*(11), 115504. https://doi.org/10.1088/2053-1591/ad09a6

Conference Proceedings and Presentations

1. Oppek, P., Goosmann, T., Reshetenko, T., Weber, A. (2023, July 4-7). *Spatial distribution of loss processes along the gas channels of PEMFC*. European Fuel Cell Forum, Lucerne, Switzerland.
2. Oppek, P., Geörg, M., Goosmann, T, Reshetenko, T. V., Weber, A., Krewer, U. (2022, May 29-June 2). *Spatially resolved deconvolution of loss processes in PEM fuel cells*. 241st Electrochemical Society Meeting, Vancouver, BC, Canada.

References

[1] Muirhead, D., Banerjee, R., Lee, J., George, M. G., Ge, N., Liu, H., Chevalier, S., Hinebaugh, J., Han, K., & Bazylak, A. (2017). Simultaneous characterization of oxygen transport resistance and spatially resolved liquid water saturation at high-current density of polymer electrolyte membrane fuel cells with varied cathode relative humidity. *International Journal of Hydrogen Energy*, *42*(49), 29472–29483. https://doi.org/10.1016/j.ijhydene.2017.10.031

2.1d Contaminant Removal and Mitigation

Continued advancement of purification technology is critical to the use of fuel cell technology under harsh environmental conditions. HNEI's previous research on gas contaminants has shown both SO_2 and H_2S to significantly impact fuel cell performance compared to most gas contaminants, due to the irreversible binding of the two contaminants to fuel cell components. In previous work, HNEI conducted contaminant absorption performance testing of novel sorbents. Recent efforts have included the synthesis and characterization of novel metal-containing ionic liquids (MIL) of type $M_x[OAc]_y[C_2mim]_z$. This research showed the 5 wt% $Mg_4[OAc]_{10}[C_2mim]_2$ activated carbon composite to have the best breakthrough performance with an SO_2 breakthrough capacity of 215 mg SO_2/g ionic liquid, which was comparable to the state-of-the-art $[C_2mim][OAc]$ ionic liquid impregnated onto activated carbon (214 mg SO_2/g ionic liquid) impregnated at similar levels.

In this work, detailed SO_2 gas sorption testing of the $Mg_4[OAc]_{10}[C_2mim]_2$ activated carbon composite sorbent under varying the environmental conditions including humidity, flow rates and gas concentration was conducted. A challenge condition including 10 ppm of SO_2, relative humidity of 50%, 1.5 LPM and a temperature of 28°C was used. As expected, higher SO_2 concentrations resulted in faster breakthrough times (Figure 2.1d.1). The same trends were observed with the changes in flow rates, as lower flow rates had relatively higher breakthrough capacities (Figure 2.1d.2). Changes in humidity caused more intriguing results. Higher relative humidity (RH) was found to have a positive effect on gas sorption, with significantly higher breakthrough times seen with 80% RH vs 50% RH (Figure 2.1d.3).

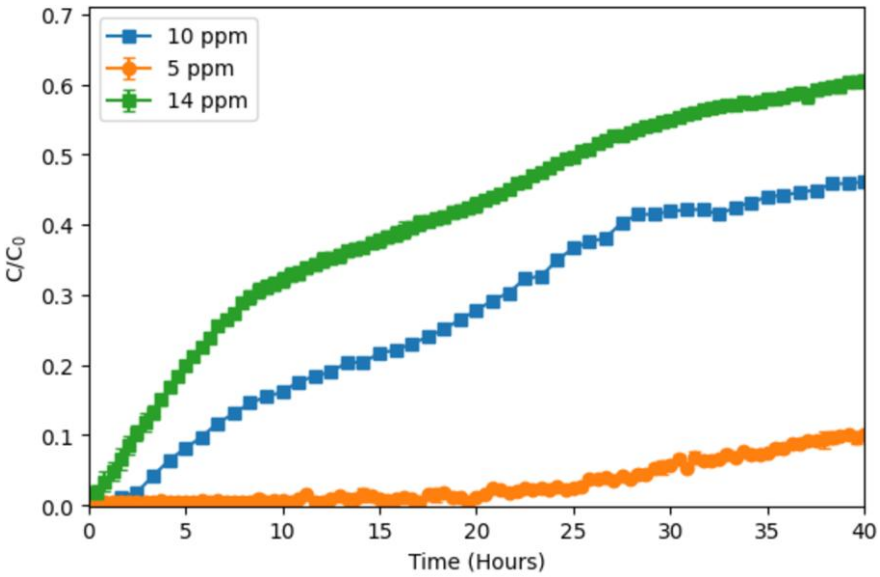

Figure 2.1d.1. The SO_2 breakthrough curves for $Mg_4[OAc]_{10}[C_2mim]_2$-activated carbon composite at different challenge gas concentrations.

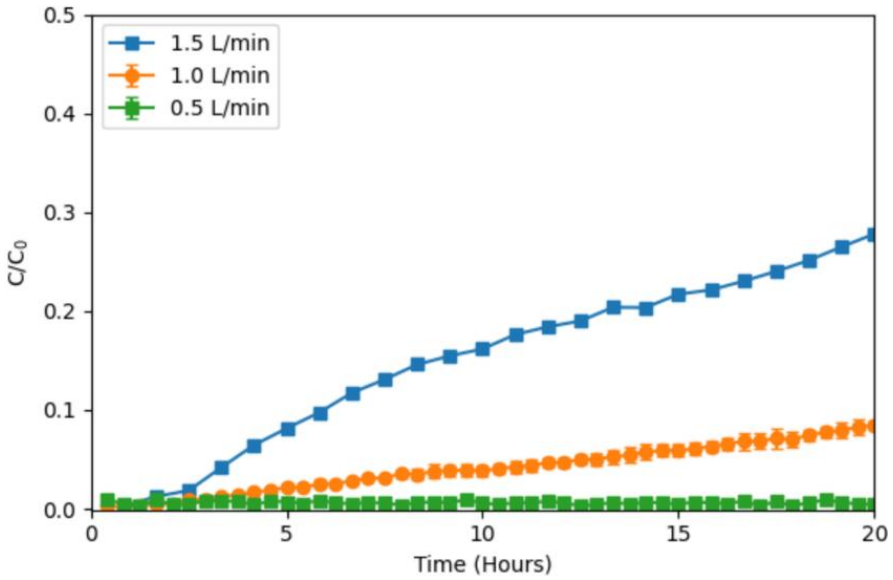

Figure 2.1d.2. The SO_2 breakthrough curves for $Mg_4[OAc]_{10}[C_2mim]_2$-activated carbon composite at varied flow rates.

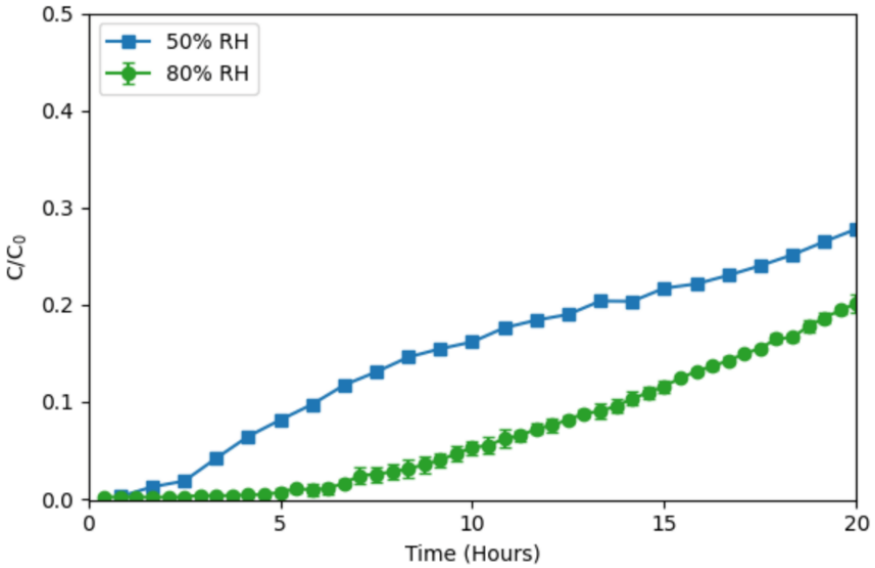

Figure 2.1d.3. The SO_2 breakthrough curves for $Mg_4[OAc]_{10}[C_2mim]_2$-activated carbon composite at 50% and 80% relative humidity.

A preliminary comparative materials cost analysis of the $Mg_4[OAc]_{10}[C_2mim]_2$ activated carbon composite versus one of the best performing ionic liquids for SO_2 sorption, $[C_2mim][OAc]$, suggests cost savings with $Mg_4[OAc]_{10}[C_2mim]_2$ (Table 2.1d.1). From a material basis, the $Mg_4[OAc]_{10}[C_2mim]_2$ composite is significantly less costly than $[C_2mim][OAc]$, and therefore, could be a better alternative in SO_2 capture since both sorbents have a similar SO_2 sorption breakthrough performance of about 215 mg SO_2/g ionic liquid.

Table 2.1d.1. Materials cost analyses for $Mg_4[OAc]_{10}[C_2mim]_2$ and $[C_2mim][OAc]$ ionic liquids.

	Material	Quantity/kg	Unit Price ($/kg)	$/g
Starting Materials	$Mg(OAc)_2$	500	14.90	0.0149
	$[C_2mim][OAc]$	500	238.43	0.238
Synthesized MIL	$Mg_4[OAc]_{10}[C_2mim]_2$			**0.08**
State of art IL for price comparison	$[C_2mim][OAc]$			**0.24**

A manuscript describing this work is currently being prepared for submission to a peer-reviewed journal. A citation and link to this publication will be accessible at https://www.hnei.hawaii.edu/publications/project-reports/aprises-21/ when available.

Publications and Presentations

Peer-Reviewed Publications

1. Abella, C., Kotsol, I., & Severa, G. Acidic Gas Sorption Performance Studies of Novel Metallo Ionic Liquid: $Mg_3[OAc]_8[C_2mim]_2$. *In preparation*.

2.2 Battery Characterization and Modeling

The research conducted under the APRISES21 Battery Characterization and Modeling subtask continued the efforts initiated under previous APRISES awards towards the improvement of data-driven approaches to characterize performance and lifetime of next generation lithium-ion batteries for both DOD and commercial deployments. HNEI used *in-silico* dataset generation in conjunction with the mechanistic battery modeling framework to test different strategies towards diagnosis and early prognosis. The emphasis for APRISES21 funding was set on complex duty cycles and a proof-of-concept study forecasting the degradation of batteries directly connected to photovoltaic systems. The work was conducted at HNEI's PakaLi Battery Laboratory on the University of Hawai'i Mānoa campus. Key accomplishments and details of the work conducted were published and are summarized below. The associated two publications are also referenced at the end of this section.

Photovoltaics supply a growing share of power to the electric grid worldwide. To mitigate resource intermittency issues, these systems are increasingly being paired with electrochemical energy storage devices, such as Li-ion batteries, for which ensuring long and safe operation is critical. However, in this operational framework, secondary Li-ion batteries undergo sporadic usage, which prevents the application of standard diagnostic methods. In Dubarry *et al.* (2023), we proposed a diagnostic methodology that used machine learning algorithms trained directly on data obtained from photovoltaic charging of Li-ion batteries (Figure 2.2.1). The training was carried out on

synthetic voltage data at various degradation conditions calculated from clear sky model irradiance data. The method was validated using synthetic voltage responses calculated from plane of array irradiance observations for a photovoltaic system located in Maui, HI, USA. We reported an average root mean square error of 2.75% obtained for more than 10,000 different degradation paths with 25% or less degradation on the Li-ion cells for days with 50% or more clear skies.

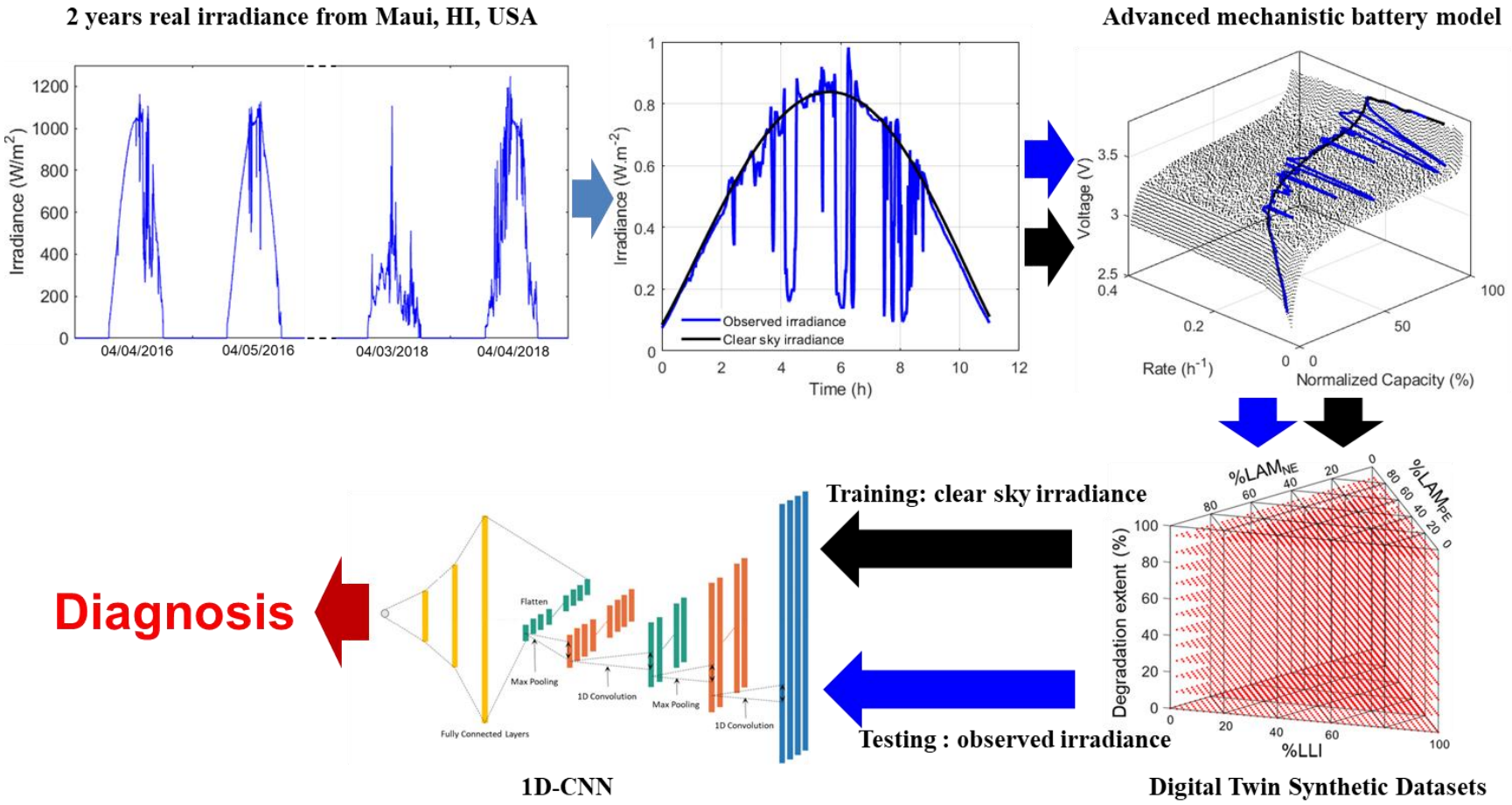

Figure 2.2.1. Schematic approach of our methodology.

In our following work, Yasir *et al.* (2025), we addressed the two main limitations of the initial approach by adding the impact of additional battery usage during charge as well as the voltage variation introduced by large battery packs. This work showed that, for capacity-based diagnosis, these limitations have a limited impact of the diagnosis accuracy and that they can be accommodated without adding much complexity by subtracting an average usage from the clear sky irradiance and by accounting for a medium level of inhomogeneities. These accommodations, while of limited impact for the average capacity-based diagnosis with around 1% increase of the average RMSE for the best-case figure, significantly improved the worst Q-based diagnoses and all the time-based diagnoses by up to 5% depending on the conditions (Figure 2.2.2).

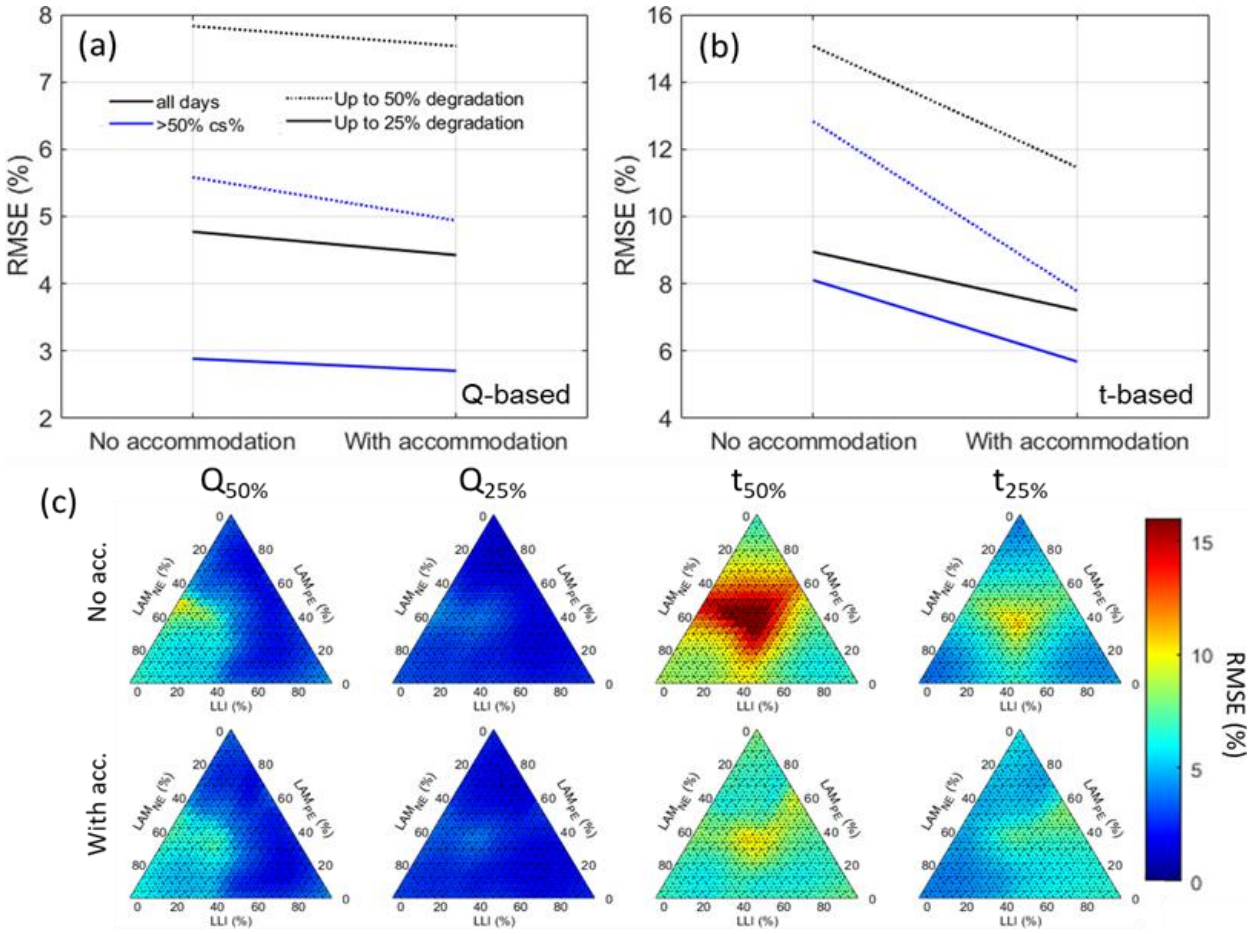

Figure 2.2.2. Effect of the accommodation on the average RMSE for (a) the Q-based diagnosis and (b) the t-based ones. (c) Diagnosis accuracy for days with >50% cs% as a function of the degradation path for simulation without accommodation (top row) and with accommodation (bottom row).

Overall, these studies reinforced the potential of synthetic data generation and training to enable big-data studies of the behavior or deployed system that will experience sporadic usage. More detail on this work can be found in the *Nature Communications* and *Batteries* publications listed below.

Publications and Presentations

Peer-Reviewed Publications

1. Dubarry, M., Costa, N., & Matthews, D. (2023). Data-driven direct diagnosis of Li-ion batteries connected to photovoltaics. *Nature Communications*, *14*(1). https://doi.org/10.1038/s41467-023-38895-7
2. Yasir, F., Sepasi, S., & Dubarry, M. (2025). Big Data Study of the impact of residential usage and inhomogeneities on the diagnosability of PV-connected batteries. *Batteries*, *11*(4), 154. https://doi.org/10.3390/batteries11040154

2.3 Printable Electronic Materials

The major objective of work under this subtask was evaluation of the functional robustness of transparent-conductive-flexible composites (TCFC) when applied to non-planar geometries or subjected to thermal stress. Specifically, the first milestone aimed to quantify the electrical conductivity of TCFCs integrated over curved or irregular surfaces, with a target of retaining at least 50% of the conductivity measured on flat substrates. The second milestone focused on assessing the mechanical durability of free-standing TCFCs, with performance benchmarks set to ensure that electrical conductivity does not degrade by more than 50% after 24 hours of exposure to 100°C and/or after undergoing 100 bending cycles. These goals were established to validate TCFCs as viable multifunctional capping layers in challenging thermal and mechanical environments.

The following presents the outcomes of our investigation into TCFCs as a multifunctional protection strategy for energy, naval, and aerospace components. The study expands the material system's utility from rigid planar substrate encapsulation to non-planar applications, specifically targeting curved or flexible systems exposed to high temperatures. Experimental efforts were guided by the two key milestones above, focusing on assessing the electrical performance and mechanical durability of TCFCs under either thermal or bending stress.

The research team at the Hawai'i Natural Energy Institute's Thin Films Laboratory is developing a new type of polymer composites integrating multi-functionalities relevant to both ONR's *Functional Polymer and Organic Materials* and *Polymer Matrix Composites* technology areas. The multi-functionalities of these composites include resistance against corrosion and having lightweight and flexibility, tunable dielectric-optical-electrical characteristics, as well as conformability to complex shapes. This technology, henceforth referred to as transparent-conductive-flexible composites (TCFC), consists of particles with specific material properties (e.g., semiconducting or metallic) protruding out of a transparent non-conductive matrix (Figure 2.3.1, left). Unlike other conductive flexible polymers, where conductive media are coated on top of the substrate, providing only in-plane conductivity, TCFCs innovate by permitting

simultaneously optical transparency and out-of-plane conductivity. Our team has thus far been successful in fabricating freestanding layers using 50 micron metallic particles embedded in hardened epoxy with both high optical transmittance (>90% in the UV(250nm)-IR(2500nm) region) and high out-of-plane conductivity (R<0.2 $\Omega \cdot cm^2$), out-performing commercial transparent conductive substrates. Recent mapping of TCFCs at the nanometer scale using atomic force microscopy in both topographic (Figure 2.3.1, center) and electrical (Figure 2.3.1, right) modes revealed that indeed electric current flows through the conductive spheres, and not the insulating polymer.

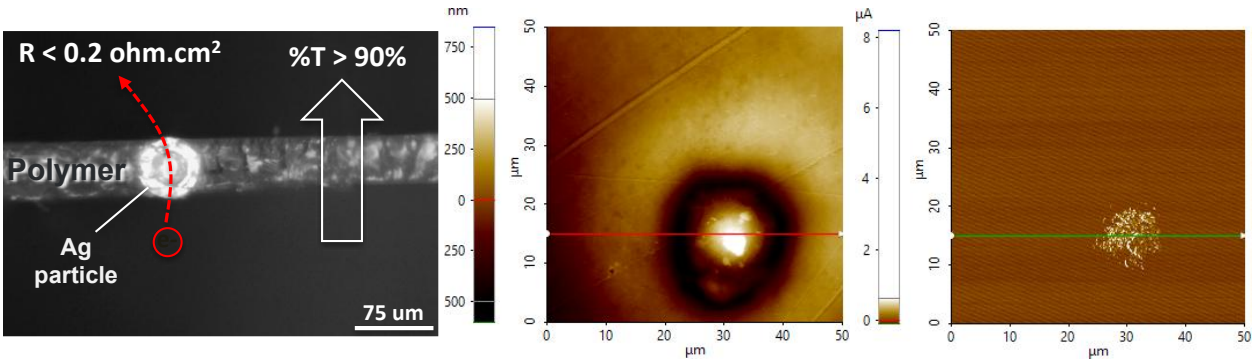

Figure 2.3.1. Cross-sectional microscopic view of a transparent-conductive-flexible composite made of 50-micron silver spheres protruding out of a flexible polymer (left), topographic (center), and electrical (right) conductivity mappings measured at the surface of a TCFC.

Our team has demonstrated the versatility and impact of TCFCs across a range of applications requiring multifunctional encapsulation and advanced integration strategies. One notable example includes the successful bonding of fully processed thin-film solar cells to create multi-junction photovoltaic devices composed of dissimilar materials that are otherwise incompatible in conventional monolithic architectures due to thermal processing constraints. By leveraging the low-temperature processability, adhesive quality, and the conductive nature of TCFCs, we enable novel device stack-ups without compromising performance. In parallel, we have validated the use of TCFCs as transparent, conductive encapsulating electrodes for the protection of moisture- and oxygen-sensitive solid-state devices. Such characteristics are particularly attractive for organic electronic devices where TCFCs function as dual-purpose electrode and encapsulant, and in marine and aerospace components, where corrosion protection must not impede electrical grounding, cathodic protection, or electrostatic dissipation. In short, TCFCs allow active electrical interfacing with protected surfaces, offering a distinct advantage over insulating encapsulations.

Our prior developments underscore TCFCs as a hybrid material that merge barrier functionality with electrical conductivity and optical transparency. Their unique structure, comprising a flexible polymer matrix with embedded conductive fillers, makes them ideally suited for applications requiring adaptability to non-flat surfaces. To evaluate processability on curved geometries, we fabricated free-standing TCFC laminates and assessed their conformity over both concave and convex surfaces. To further explore the effect of surface modification on mechanical and electrical

performance, an additional TCFC sample was coated with a 100 nm silver thin film and subjected to an identical bending test.

As summarized in Figure 2.3.2 and Table 2.3.1, TCFC samples were able to achieve bending radii as tight as 5 mm for up to 100 bending cycles (tested so far) without compromising structural integrity and electrical conductivity. Both uncoated and silver-coated TCFC samples exhibited negligible changes in electrical resistivity after repeated bending, indicating excellent mechanical robustness and preservation of electrical pathways under flexural strain. Notably, the silver-coated TCFC showed comparable resilience, reinforcing the feasibility of incorporating functional surface treatments that enhance end-use specific performance without impairing mechanical compliance.

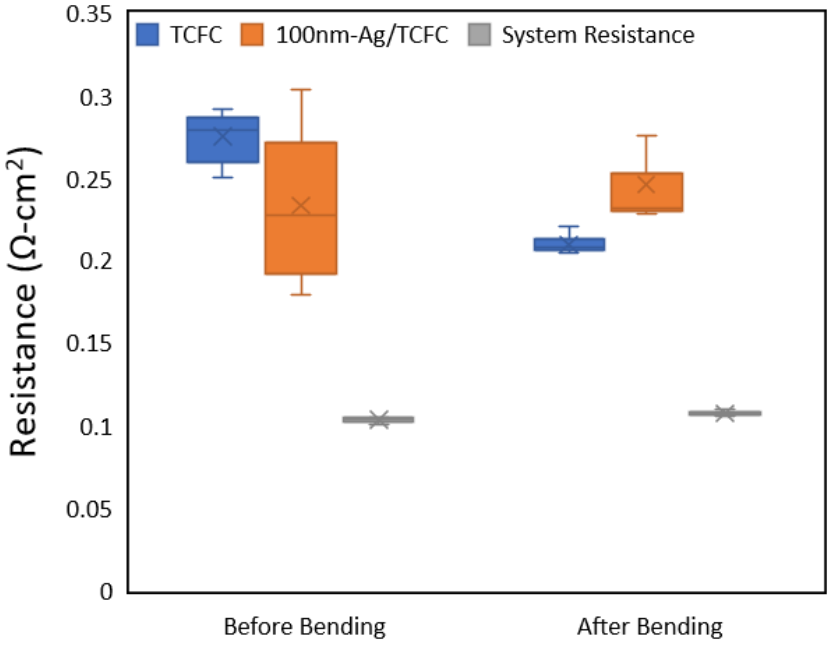

Figure 2.3.2. Summary of electrical resistance for TCFC samples, with or without 100nm Ag coating, before and after being subjected to 100 bending cycles.

Table 2.3.1. Summary of electrical resistance for TCFC samples, with or without 100nm Ag coating, before and after being subjected to 100 bending cycles.

Sample	Resistance of as-synthesized sample (Ω·cm²)	Resistance after 100 bending cycles (Ω·cm²)
TCFC	0.275	0.210
Ag-TCFC	0.233	0.246
System Resistance	0.104	0.107

Figure 2.3.3 and Table 2.3.2 summarize the electrical performances of TCFCs under thermal stress. TCFCs, synthesized from distinct room-temperature curing Aluzine epoxy and high-temperature curing (sample cured at 80°C) Masterbond epoxy, both demonstrate sustained electrical performance after 24 hours of annealing at 100°C. Collectively, these results affirm the

adaptability of TCFC systems for next-generation encapsulation strategies, especially in scenarios where simultaneous demands for environmental isolation, electrical functionality, optical transparency, and mechanical flexibility converge with heat exposure. Additional functional surface modifications open the door to custom-tailored encapsulant solutions for photovoltaics, defense, aerospace, and emerging soft electronics, and underscore their potential as a hybrid encapsulation that advances the next generation of functional surface technologies.

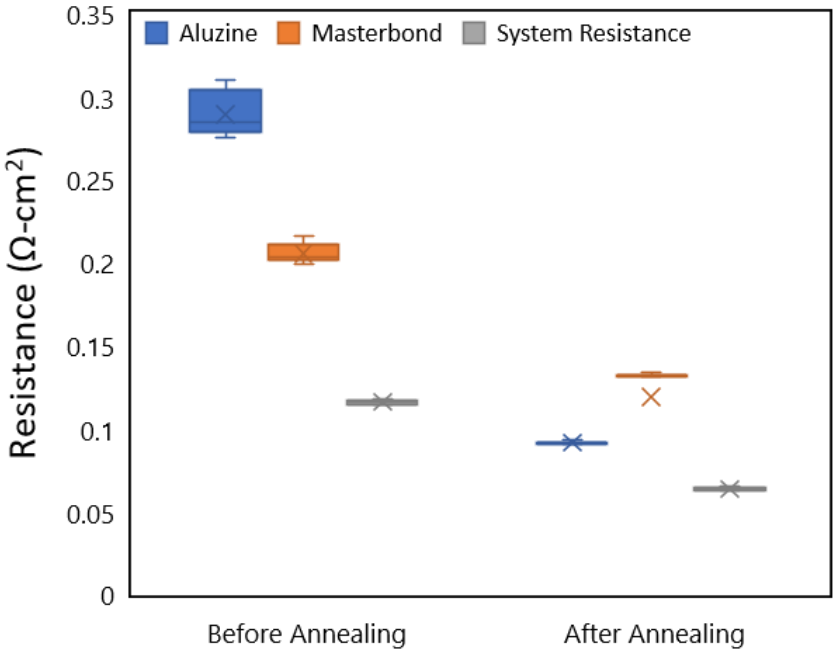

Figure 2.3.3. Summary of electrical resistance for Aluzine and Masterbond-based TCFC samples before and after being subjected to 24 hours of annealing at 100°C.

Table 2.3.2. Summary of electrical resistance for Aluzine and Masterbond-based TCFC samples before and after being subjected to 24 hours of annealing at 100°C.

Sample	Resistance of as-synthesized sample (Ω·cm²)	Resistance after 24 hours at 100 ˚C (Ω·cm²)
Aluzine	0.289	0.091
Masterbond	0.205	0.132
System resistance	0.115	0.063

TASK 3: ALTERNATIVE FUELS

Task 3 included three subtasks focused on investigation of biocarbon produced from transient plastic phase biochars, investigation of sulfur-containing compounds in marine fuels, and support of HNEI's hydrogen fueling infrastructure. Research from the first two subtasks produced a submitted manuscript currently under review to the *Energy & Fuels* journal and another paper

published in the *Fuel* journal. Subtask 3.3 supported the development, assessment, and operation of the hydrogen infrastructure and vehicles on the Big Island of Hawai‘i. Details of each research subtask are provided in the following sections.

3.1 Constant Volume Carbonization

Transient plastic phase biochars (TPPB) produced from different woody feedstocks (birch, spruce, eucalyptus) were investigated to understand the underlying factors responsible for differences in mechanical performance of biocarbon produced from these materials. All TPPB materials were produced under identical constant pressure (12.4 MPa) using wet 1-2 mm particles (75 wt% H_2O addition) and reacted for 30 minutes at 320°C under nitrogen gas. TPPB materials were analyzed using proximate analysis, thermogravimetric analysis (TGA), differential scanning calorimetry (DSC), Fourier transform infrared spectroscopy (FTIR), quantitative carbon-13 nuclear magnetic resonance (^{13}C NMR), and gas chromatography-mass spectrometry (GC-MS) of solvent extracts, while biocarbon pellets were studied by mechanical, conductivity, porosity, and CO_2 reactivity tests as well as microscopy.

Whereas the general properties of the TPPB chars were overall quite similar, several key differences were observed that provide insights into the different mechanical performance when converted to biocarbon. Specifically, the TPPB from birch contained a high concentration of triterpenoids which are not present in the TPPB from either eucalyptus- or spruce-derived TPPB. Pronounced differences in the ^{13}C NMR spectra and TGA thermograms reflect this additional component that is not present in the eucalyptus and spruce.

Results from this study suggests that the superior mechanical performance of biocarbon produced from birch TPPB likely results from the triterpenoids acting as plasticizing agents that alter the glass transition temperature of the material. This results in more inter-particle bonding to occur during calcination increasing the mechanical strength of the resulting biocarbon.

A manuscript describing this work was submitted to the *Energy & Fuels* journal. It is currently undergoing peer review. A citation and link to this publication will be accessible at https://www.hnei.hawaii.edu/publications/project-reports/aprises-21/ when available.

3.2 Marine Fuels

Sulfur-containing compounds (SCCs) are the most abundant heteroatomic organic species (HOS) in petroleum fuels. This subtask investigated the dynamics of SCCs in surrogate fuel systems,

focusing on their oxidation stability, reactivity, and interactions. An analysis of eleven selected SCCs, spanning both reactive (thiols, sulfides, and disulfides) and nonreactive (thiophenes and benzothiazole) species, was conducted at 140°C. The investigation delved into reaction and degradation mechanisms, exploring resulting products, binary mixtures of reactive SCCs for potential interactions, and multicomponent SCC systems to understand nuanced interaction.

Findings revealed unique reaction pathways in single-component SCCs, synergetic and antagonistic effects in binary mixtures, and substantial decreases in reaction rates in all multicomponent systems. Moreover, SCCs expedited antioxidant consumption, highlighting their pivotal role in fuel stability and degradation. The study contributes valuable insights into SCC dynamics, advocating further exploration of HOS's interactions for enhanced fuel formulation and stability testing strategies.

More detail on this work can be found in the *Fuel* publication listed below.

Publications and Presentations

Peer-Reviewed Publications

1. Fu, J., & Turn, S. Q. (2025). Oxidation mechanism of sulfur-containing compounds and antioxidant depletion dynamics: Insights into interactions. *Fuel*, 381, 133341. https://doi.org/10.1016/j.fuel.2024.133341

3.3 Hydrogen Refueling Technology

The Hawai‘i Hydrogen Power Park ("Power Park") was established in 2003 to support the U.S. Department of Energy's (DOE) Technology Validation Program. The Power Park was funded by the DOE through the Department of Business, Economic Development and Tourism's Strategic Industries Division (DBEDT), with the Hawai‘i Natural Energy Institute (HNEI) at the University of Hawai‘i serving as the implementing partner. This effort conducted engineering and economic validation of pre-commercial hydrogen technologies. Power Park Phase 1 systems included a commercial scale grid-connected alkaline electrolyzer interfaced with a gas storage system and a 5 kW proton exchange membrane (PEM) fuel cell located at the Hawai‘i Fuel Cell Test Facility (HFCTF) in Honolulu.

Power Park Phase 2 was proposed to expand the capabilities of the Power Park through the testing and validation of hydrogen fueling system technologies on the Big Island of Hawai‘i. In parallel, the Hawai‘i Volcanoes National Park (HAVO) had been selected for funding through the Advanced Transportation for Parks and Public Lands (ATPPL) program by the Department of Transportation (DOT) via the Department of Interior (DOI) to purchase two hydrogen-hybrid shuttle buses for tours of the park. The project was intended to support HAVO's hydrogen fueling requirements leveraging

additional investment from the State of Hawai‘i’s Hydrogen Investment Capital Special Fund (“Hydrogen Fund”). In its initial formulation, the Department of Defense (DOD), through the Kilauea Military Camp (KMC), offered to serve as the host site for the fueling infrastructure for the vehicles.

While initially targeted for installation at the HAVO site, concern about environmental issues in the National Park resulted in a site change to the Puna Geothermal site. In this configuration, support for the HAVO vehicles was to be provided by leveraging a hydrogen production system installed at the Puna Geothermal Ventures (PGV) power plant utilizing renewable electricity produced at the geothermal plant to produce electrolytic hydrogen. The hydrogen was to be delivered to HAVO by tube trailer and dispensed to the HAVO vehicles from a dispenser located at the KMC site.

In 2010, in response to Navy’s interest in the use of fuel cell vehicles to achieve higher vehicle efficiency and to lower fuel use, HNEI collaborated with the Naval Research Laboratory (NRL), proposing a collaborative project to DOE to investigate the potential for the intermittent operation of a grid-connected electrolyzer to produce hydrogen and provide grid services for large-scale electric grid applications. NRL served as the technical lead and overseer of the hydrogen production program with HNEI serving as the implementing partner. Ultimately, community concerns with the PGV site resulted in a final siting at the Natural Energy Laboratory Hawai‘i Authority (NELHA) site in Kona, Hawai‘i.

The PGV/NELHA hydrogen production system was procured under Award N00173-10-1-G037, P00001 through NRL. The stated objectives of the project were to optimize use of the electrolyzer and hydrogen storage system and utilize the hydrogen for transportation while also allowing greater penetration of variable renewable generation sources onto the grid, and to reduce barriers to the introduction of the hydrogen infrastructure. The variable hydrogen production was intended to support load leveling of the electricity produced by variable renewable energy sources such as wind, solar, and geothermal on the Big Island of Hawai‘i. Hydrogen produced from the system was also intended to be used as a transportation fuel.

Under this agreement with NRL, HNEI conducted cyclic testing of the hydrogen production system at Powertech Labs, located in Vancouver, Canada, to characterize the dynamic response of the system. Following modification of the system controls, it was installed at NELHA on the Island of Hawai‘i.

In addition to conducting the research to characterize and control the variable load to provide grid services, additional goals included:

1. Support hydrogen vehicle demonstration projects on the Big Island of Hawai‘i;
2. Conduct technical analysis of system and subsystem performance in a real-world environment; and

3. Document liability, insurance, and permitting issues and their resolutions.

As illustrated in Figure 3.3.1, the concept was to produce fuel cell grade hydrogen at NELHA to be delivered to the Mass Transit Agency (MTA) base yard in Hilo to support heavy-duty FCEBs operated by the MTA Hele-On public bus service. Three trailers each with a capacity of 105 kg were procured for transporting hydrogen between the production and fueling site. The trailers were certified by the Federal Transit Administration Department of Transportation for use on U.S. public roads.

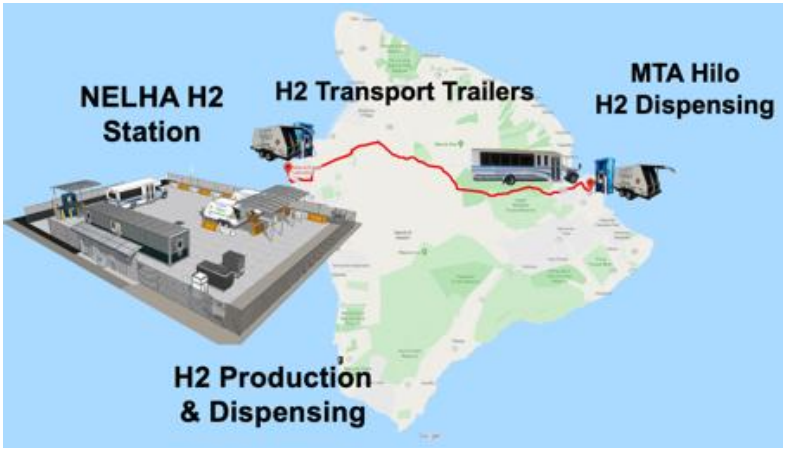

Figure 3.3.1. Concept diagram of the transportation of hydrogen on the Big Island of Hawai'i.

These investments collectively supported workforce development, operations, and research activities within Hawai'i's unique island environment.

At the core of this project was Hawai'i's first public hydrogen fueling station, commissioned at NELHA. The station utilizes a Nel (formerly Proton Onsite) 65 kg/day PEM electrolyzer to produce ultra-pure hydrogen at 30 bar (440 psi). A Hydro-Pac compressor increases this pressure to 438 bar (6,352 psi). Hydrogen fueling occurs at a nominal 350 bar (5,000 psi) through fully automated dispensers equipped with advanced safety interlocks and fail-safe mechanisms, supported by redundant underground piping and specialized interfaces designed specifically for these hydrogen transport trailers (Figures 3.3.2, 3.3.3, and 3.3.4). Previous work revealed issues with control system responsiveness and software reliability, leading to a complete redevelopment of fueling control software and operational protocols—a process that granted HNEI full technical autonomy over its hydrogen dispensing systems.

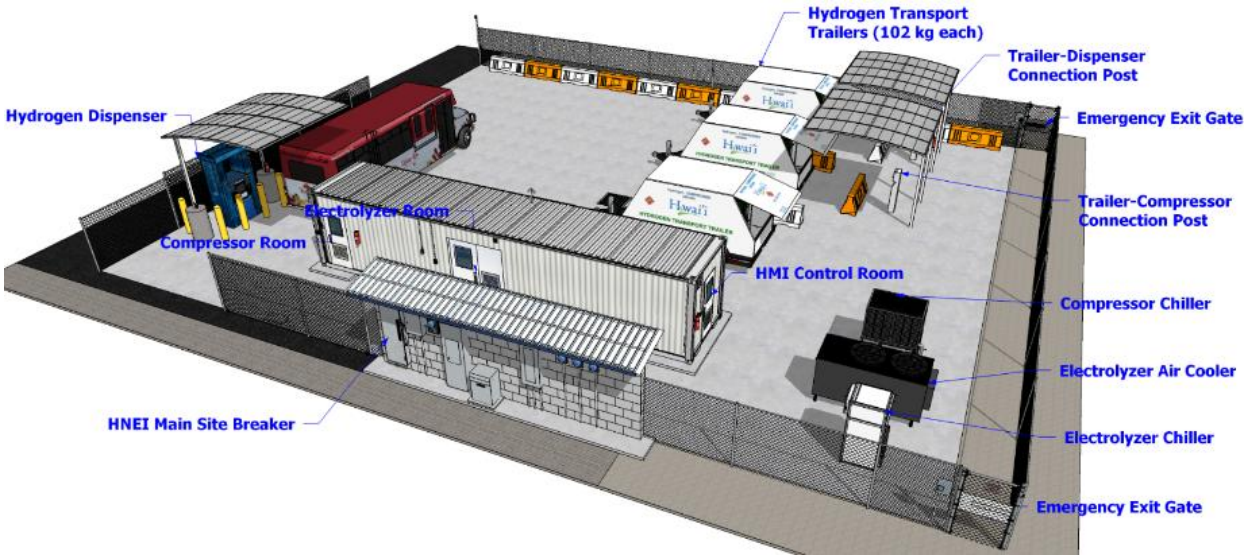

Figure 3.3.2. Major components of Hawai'i's first hydrogen fueling station at NELHA.

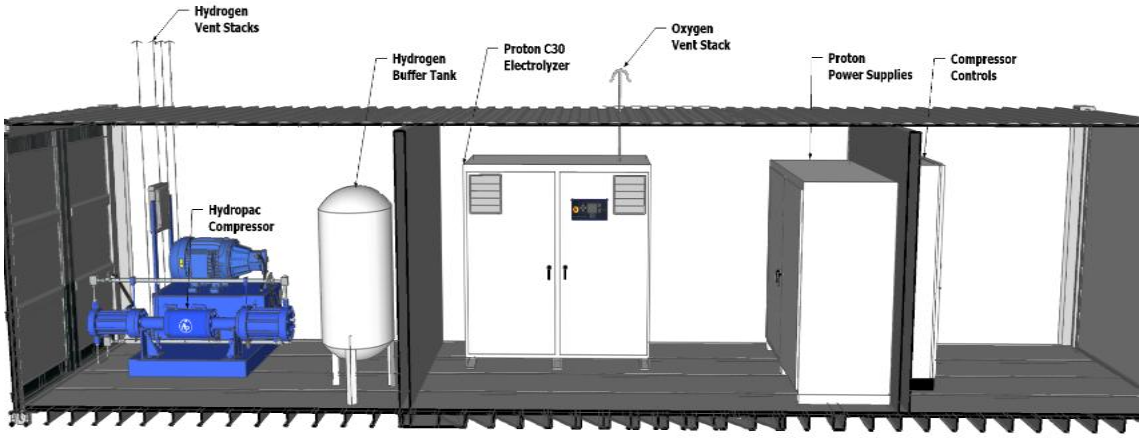

Figure 3.3.3. The components inside the shipping container.

Proton onsite C30 electrolyzer

Hydro-Pac compressor

Powertech/HNEI mobile hydrogen tube trailer

Figure 3.3.4. Process flow illustrating hydrogen being produced on site through water electrolysis and then compressed to 450 bar and stored in mobile hydrogen tube trailers.

During the initial bus deployment phase, HNEI played a critical role supporting U.S. Hybrid's startup and integration of the 21-passenger hydrogen fuel cell electric bus, resolving a range of technical challenges such as optimizing fuel cell battery charging, algorithms to allow safe

charging at stoplights, mitigating DC-to-DC converter fuse failures through hardware and software improvements, and enhancing thermal management via increased radiator fan speeds at low bus speeds. Additional efforts included troubleshooting sensor interference, repairing drivetrain components, and addressing cooling system leaks, enabling the bus to enter reliable daily service routes where it demonstrated impressive performance metrics of approximately 1.2 kWh energy consumed per mile and 12.7 miles per kilogram of hydrogen over 145-mile runs.

Operating in close proximity to Hawai‘i’s marine environment posed additional technical challenges. The team developed an aggressive program to address corrosion caused by the coastal salt-air atmosphere that included selecting corrosion-resistant materials and refining maintenance schedules.

In addition to station development, HNEI supported the retrofit and deployment of two fuel cell electric buses (FCEBs) in the County of Hawai‘i’s Hele-On fleet. The primary vehicle (Figures 3.3.5 and 3.3.6) is a 21-passenger ADA-compliant bus designed and converted by U.S. Hybrid, powered by dual 11 kWh lithium-ion batteries, a 200 kW drivetrain, and a 40 kW fuel cell (upgraded from the original 30 kW). This bus also integrates a 10 kW export power system capable of sustaining emergency AC power for up to 30 hours on a single hydrogen fill—an innovation enhancing community resilience in emergencies or extended power outages. The secondary platform is a 19-passenger bus originally intended to serve Hawai‘i Volcanoes National Park that was upgraded with a 90 kW Hyundai fuel cell and an expanded 33 kWh battery pack to enable service on Hawai‘i’s more challenging topographic routes.

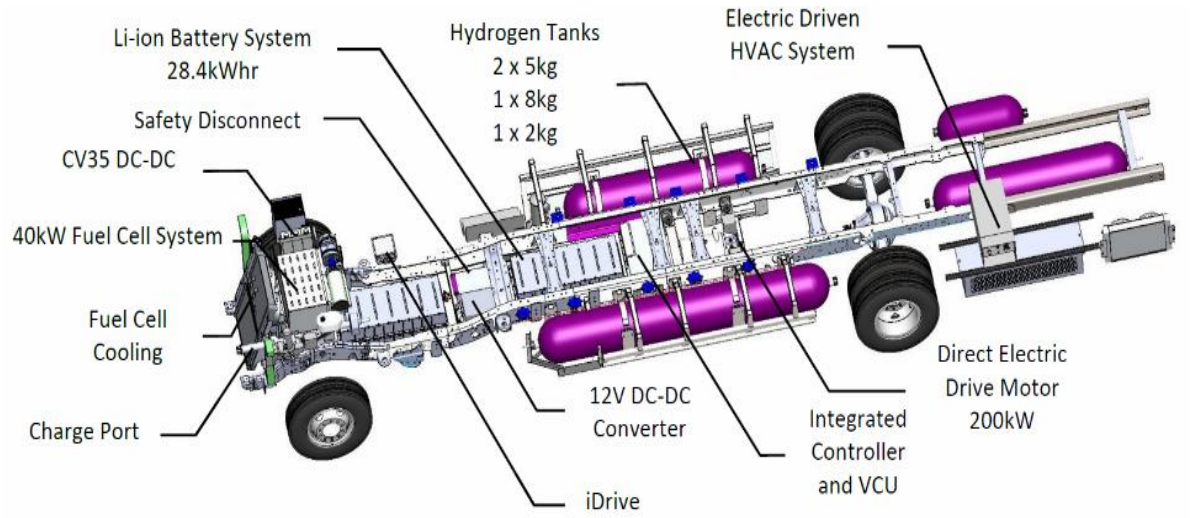

Figure 3.3.5. Components of a hydrogen fuel cell bus.

Figure 3.3.6. Hele-On Bus refueling at the 350 bar hydrogen dispenser.

Advanced data collection systems for bus and station operations were developed (Figure 3.3.7).

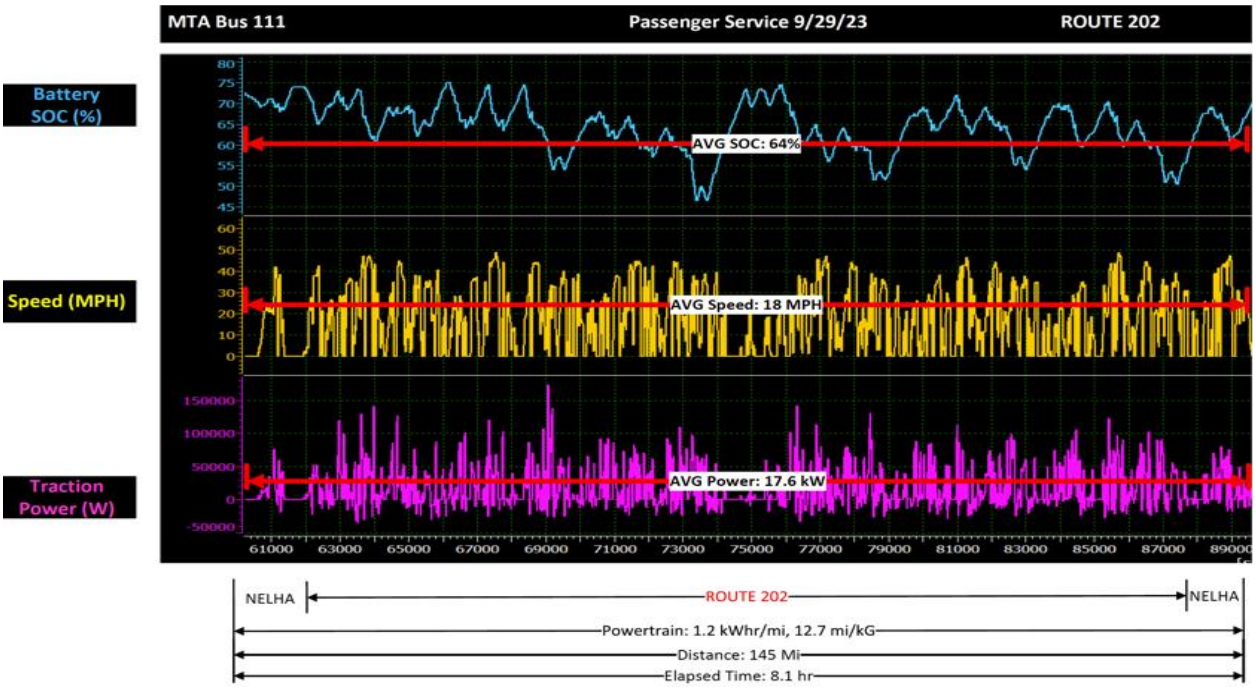

Figure 3.3.7. Telemetry data from the buses.

Under these programs, HNEI developed and delivered training modules tailored for bus operators, maintenance technicians, emergency responders, and fueling station staff. These programs included classroom instruction, hands-on equipment familiarization, and emergency drills, building a robust, locally based cadre of hydrogen-qualified personnel poised to sustain and expand hydrogen transit operations.

Community and stakeholder engagement included tours (Figure 3.3.8), briefing sessions, public demonstrations, and educational programs enriching local understanding and support.

Figure 3.3.8. Tour of the hydrogen station.

The program maintained comprehensive hydrogen station operational and safety documentation, including the operations manual, safety management plan, emergency response plan, standard operating procedures, and hazardous material and waste management program to ensure safe and reliable station and fleet.

In 2024-2025, HNEI initiated a transition of the assets to another state agency, NELHA, for continued use and development. With the closure of U.S. Hybrid's local operations in 2024, the program assumed full responsibility for station system controls and maintenance. Hydrogen trailers were decommissioned. As of the publication of this report, negotiations with NELHA are ongoing with transfer expected to occur in late 2025 or early 2026.

Overall, the project has achieved several key goals:

- *End-to-End Hydrogen System Deployment*: Designed, demonstrated, commissioned, and operated Hawai'i's first public PEM-based refueling station, integrated with County bus operations;
- *Transit Fleet Integration*: Deployed and upgraded buses, and documented bus performance (efficiency, range, maintenance);
- *Technical Feasibility and Innovation*: Collected operational data at both station and bus levels, developed in-house control systems and manuals, and proved hydrogen transit viable under island conditions;
- *Workforce Development*: Trained dozens of drivers, mechanics, and first responders with sustained funding from FTA to ensure future pipeline capacity; and

- *Public/Stakeholder Engagement*: Conducted tours, workshops, community events, and policy briefings, strengthening Hawai‘i’s role in global hydrogen collaboration.

During the development and operation of the facility and buses, funding from four awards by the Office of Naval Research (ONR): APRISES20 (N00014-21-1-2250), APRISES21 (N00014-22-1-2045), APRISES22 (N00014-23-1-2720), and APRISES23 (N000142412397) were used to support the operation and maintenance of the fueling infrastructure and collect data from the hydrogen fuel cell electric buses (FCEBs). These ONR funds leveraged ongoing support from the State of Hawai‘i and the County of Hawai‘i.

Key contributions supported by APRISES21 funding included:

- Completed full operational commissioning of the NELHA hydrogen station’s primary systems (electrolyzer, compressor, dispenser), achieving steady production of 65 kg/day hydrogen with infrastructure designed to scale to 120 kg/day;
- Weight certified tube trailers and hydrogen purged the three tube trailers to prepare them for operation;
- Deployed and operated three DOT-certified hydrogen transport trailers for fuel delivery;
- Repaired compressor chiller coil leak, overhaul of 438 bar Hydropac compressor and completed first compressor run;
- Enhanced station reliability and safety through equipment upgrades and preventative maintenance, including hydrogen sample testing and troubleshooting; replacement of electrolyzer sensors, water filtration pump, HMI PC, and tube trailer pressure transducers; installation of a Shark energy meter; and addition of a dispenser hose mesh covering;
- Established automated hydrogen dispensing systems with fail-safe controls to ensure reliable station and bus fueling operations;
- Demonstrated a 15% increase in fuel cell power (from 40 kW to 46 kW) and a 50% increase in bus range (from 200 to 300 miles);
- Supported the County of Hawai‘i Mass Transit Agency’s acquisition of two 19-passenger FCEBs from Hawai‘i Volcanoes National Park and supported upgrade to 40 kW fuel cells and A123 lithium-ion batteries;
- Participated in the U.S. DOE-sponsored “H2 Twin Cities” initiative fostering global hydrogen collaboration;
- Presented at the Hawai‘i Energy Conference and hosted the “Meet the Bus” (Figure 3.3.9) launch event, attended by over 100 community members;

Figure 3.3.9. "Meet the Bus" event on Hawai'i Island

- Delivered multiple briefings and tours of the HNEI hydrogen station to stakeholders including the Center for Transportation and Environment (CTE), State of Hawai'i Department of Transportation, Pacific Hydrogen Alliance, Kamehameha Schools, Stanford University students, and emergency preparedness organizations; and
- Advanced community and professional knowledge of hydrogen infrastructure through targeted outreach and educational programs, including engagements at the National Disaster Preparedness Training Center.

Publications and Presentations

Peer-Reviewed Publications

1. Ku, A. Y., Kocs, E. A., Afzal, S., Ewan, M., Glenn, J. R., Toma, F., Vickers, J., Weeks, B., & White, A. A. (2023). Opportunities for the materials research community to support the development of the H2 economy. *MRS Energy & Sustainability*, 10(2), 158–173. https://doi.org/10.1557/s43581-023-00061-3

TASK 4: RESILIENT ENERGY SYSTEMS

Under Task 4, HNEI proposed to continue research to enable high penetration of variable renewable generation technologies while maintaining resilient, reliable, and secure energy systems. The proposed work included two closely integrated activities. Under Subtask 4.1, HNEI continued development of enabling technology focused on the integration of new technology and reliable control at the grid edge. Subtask 4.2 focused on power systems analysis with a focus on resource risk assessment to ensure that the energy systems and related critical infrastructure on O'ahu and the other Hawaiian Islands, home to the Pacific Command and the largest military bases in the Asia Pacific region, meets the reliability needs of DOD as significant amounts of variable

generation technologies are integrated into the grid. Details of each research subtask are provided in the following sections.

4.1 Advanced Grid Technology

HNEI's Grid System Technologies Advanced Research Team (Grid***START***) completed work under this subtask. Leveraging previous funding and partnerships across Hawai'i and the Asia Pacific region, HNEI's research continues to advance, demonstrate, and validate efficient grid performance, reliability, and resilience with high renewable penetrations, focusing on grid edge technologies, distributed energy resources (DER), and microgrid applications. The team engaged in the following research and development projects: a) diagnosis and the resolution of communication issues between controller and inverters for an advanced conservation voltage reduction (CVR) system and devices; b) development of a holistic optimization framework for resilient, cost-effective microgrid planning and design; and c) efficiency and safety enhancements to a DC microgrid system on Coconut Island and upgrades to an electric boat's energy systems. Details of the work conducted in each of these activities are described below.

4.1a Advanced Conservation Voltage Reduction Demonstration

The primary goal of this project was to demonstrate energy efficiency through advanced conservation voltage reduction (CVR) on the distribution circuit serving the Plaza Housing complex at U.S. Marine Corps (USMC) Camp Butler in Okinawa, Japan. This project involves the development, field implementation, testing, and evaluation of grid improvement technologies.

In collaboration with USMC Facilities personnel, HNEI Grid***START*** selected the 13.8 kV "Feeder F6A" distribution circuit for the advanced CVR demonstration. This single feeder, containing approximately 56 distribution service transformers, is fed by a large substation transformer that provides power to a total of ten feeders. To maintain project scope and budget, a section of Feeder F6A that serves the Plaza Housing complex was identified for the CVR control. The CVR-controlled feeder section was isolated with a voltage regulator (VR) to manage and control the voltage at "downstream" service transformers, essentially behaving as the load tap changer (LTC) on a substation transformer, but for the limited section of the feeder under test.

Specifically, the project focuses on seven distribution service transformers at the feeder's branch end, five of which had existing advanced metering infrastructure (AMI) meters and communications. While the VR's LTC can lower the voltage profile of the entire feeder, it cannot address individual low- or high-voltage points along the feeder path. Consequently, the minimum

voltage point along the feeder path limits the voltage reduction potential achievable by the LTC for the entire feeder length. Under prior APRISES funding and to achieve greater CVR benefits across the feeder, HNEI has patented and demonstrated a method of localized voltage management using an advanced CVR device. This device uses local power measurements to: 1) smooth the voltage profile by managing and regulating the reactive power output of inverters; 2) increase voltage at the critical minimum voltage point regulated by the VR; and 3) maximize CVR benefits for all customers.

A new distribution pad-mounted VR, guided by near real-time voltage recordings, regulates the primary voltage of these seven service transformers to maintain customer service voltages at the lower limit of the ±5% American National Standards Institute (ANSI) voltage range. This implementation is expected to reduce energy consumption by 0.7% to 0.9% for every 1% voltage reduction. This is the primary value proposition of effective CVR implementation and it reduced energy use by more effective management of customer service voltage.

The project infrastructure, developed under previous APRISES funding and shown in Figure 4.1a.1, integrates both existing and new technology including:

- New VR with HNEI-developed controls (with associated bypass switch) at GS 32;
- Seven distribution service transformers serving various military base loads (e.g., Officer's Club commercial load, troop barracks, fitness gym, and single-family residential housing);
- Metering systems and mesh radio network communications;
- HNEI-developed reactive power voltage management system (advanced CVR device) installed at TH 415; and
- 5 kW photovoltaic (PV) system served by TH 415.

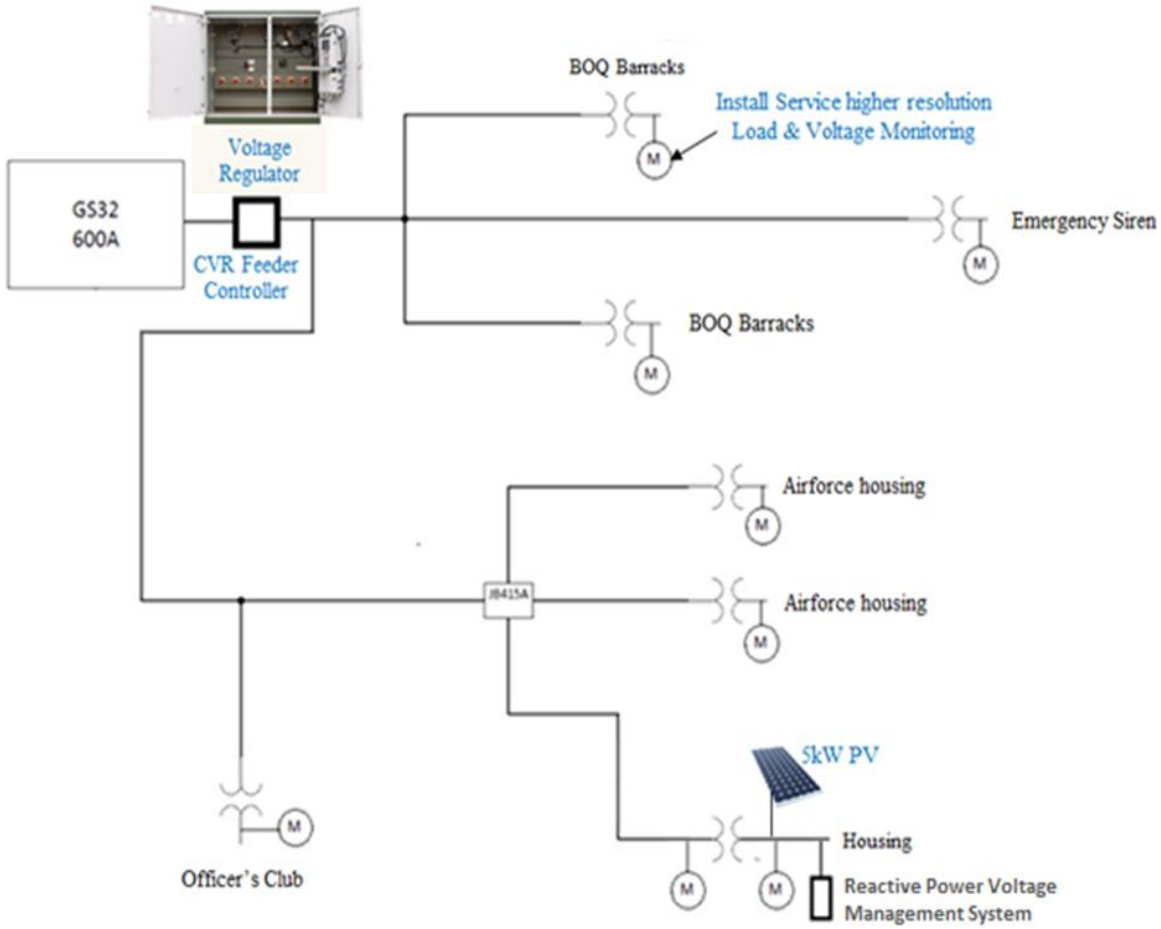

Figure 4.1a.1. Electrical one-line diagram of the project demonstration area.

The advanced CVR device manages the voltage at the TH 415 distribution service transformer, which is tied to the 5 kW PV system and served building loads. This system aims to eliminate voltage drop across the service transformer at the feeder's lowest voltage point, enabling deeper voltage turndown across the feeder and enhancing the overall performance of the CVR controller at the VR. The Volt-Var Control (VVC) algorithm incorporates an on/off schedule to assess controller effectiveness. As shown in Figure 4.1a.2, when the VVC controller is enabled, the voltage-drop across the transformer impedance (red line) decreases as controlled power inverters generate reactive power (blue line).

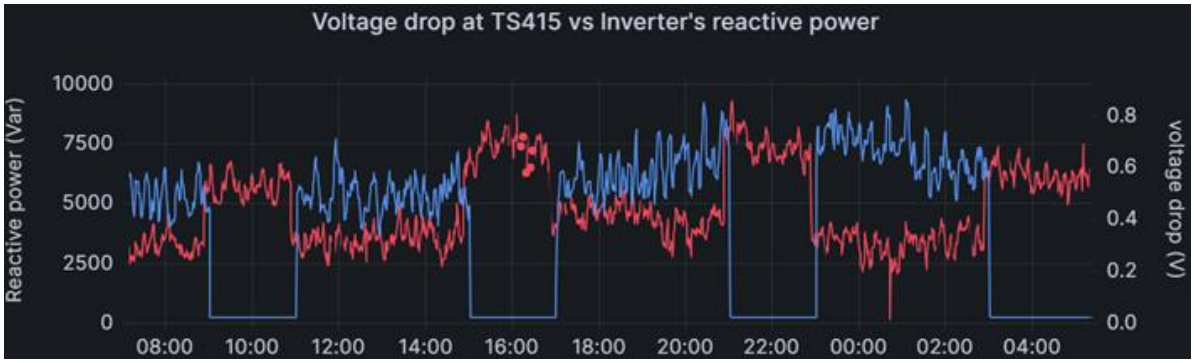

Figure 4.1a.2. Reactive power support via VVC reducing voltage drop.

Major activities completed under previous APRISES funding included:

- Validation of an advanced CVR control algorithm and field meter communications using a hardware-in-the-loop (HIL) test platform at HNEI's Advanced Power System Laboratory (APSL) on O'ahu;
- Development of a CVR algorithm and control dashboard webpage;
- Completion of electrical installation drawings and bid package for VR installation;
- Completion of major construction services with the dedicated support of the USMC General Facilities Engineering Division and Naval Construction Force's Seabees;
- Installation of underground electrical conduits and concrete pad;
- Reconfiguration of distribution circuits and VR installation;
- Resolution of AMI mesh communication system issues through antenna replacement;
- Resolution of pQube meter failures through technical modifications;
- Commissioning of VR system following COVID-19 delays;
- Field installation and operationalization of CVR system controls;
- Implementation of reactive power voltage management (advanced CVR device) at TH-415 transformer;
- Continuous improvement and maintenance of VR and associated CVR control system;
- Resolution of main control board failure at TH415 in October 2022 due to overvoltage, lightning strikes and/or overheating;
- Implementation of laboratory testing using the HIL test platform at HNEI's APSL;
- Establishment of a weekly data collection system in collaboration with USMC Camp Butler team;
- Development of a comprehensive database for evaluation of three data sources: 1) local recording of data from smart pQube meters at each distribution service transformer; 2) input and output data of the CVR controller, including VR data via DNP3 protocol and pQube meter data via Modbus TCP protocol at higher resolution; and 3) data from the VVC controller for the managed dispatch of reactive power produced by power inverters at TH 415;

- Integration of a Network Time Protocol (NTP) server for time synchronization across all data sources;
- Implementation of a fully operational advanced CVR system that autonomously manages downstream service transformer voltages through the tap changes and the VVC algorithm;
- Operation on alternating-day schedule for CVR assessment (see Figures 4.1a.3 and 4.1a.4), with the following results: 1) CVR factor for the feeder supplying the seven service transformers determined to be between 0.75% and 0.93%; 2) approximate voltage reduction of 2.25% achieved during active advanced CVR control; and 3) potential monthly energy savings of 1.82 to 2.26 MWh, based on a recorded total monthly energy consumption of 97 MWh for the seven service transformers under CVR control;
- Assessment and recovery following typhoon damage in August 2023, including high-voltage and insulation testing of VR and cables (October 2023 and January 2024), verification of VR integrity via megger test and oil analysis, and successful re-energization of the VR on April 22, 2024;
- Migration of the advanced CVR demonstration project's communication system outside the camp's AMI network to meet USMC's evolving stringency in cybersecurity requirements, completed on June 6, 2024;
- Relocation of the VVC controller and associated power meter outside TH415 in October 2024, including hardware and software upgrades, and installation of a dedicated power meter; and
- Initiation of troubleshooting efforts after the relocation and software upgrades, due to inverters (reactive power resources) not receiving commands from the VVC controller.

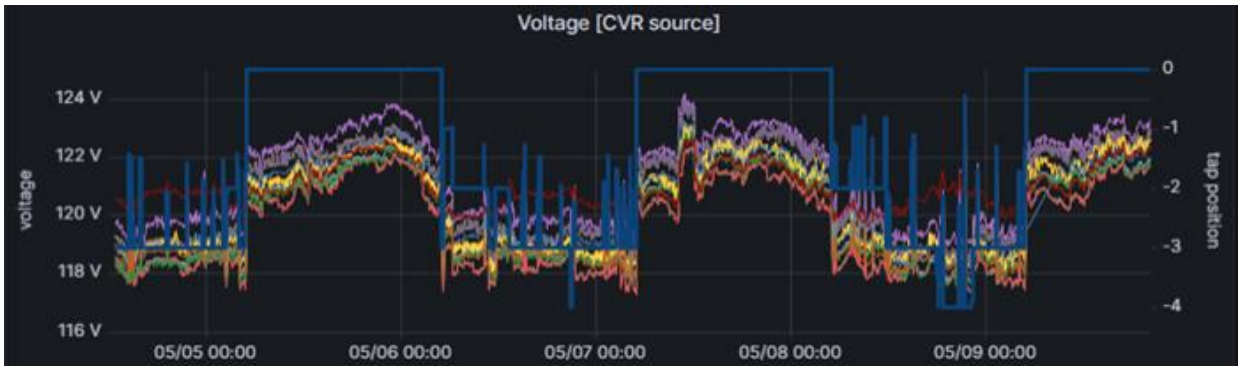

Figure 4.1a.3. Voltage profiles during on/off cycles of the advanced CVR system.

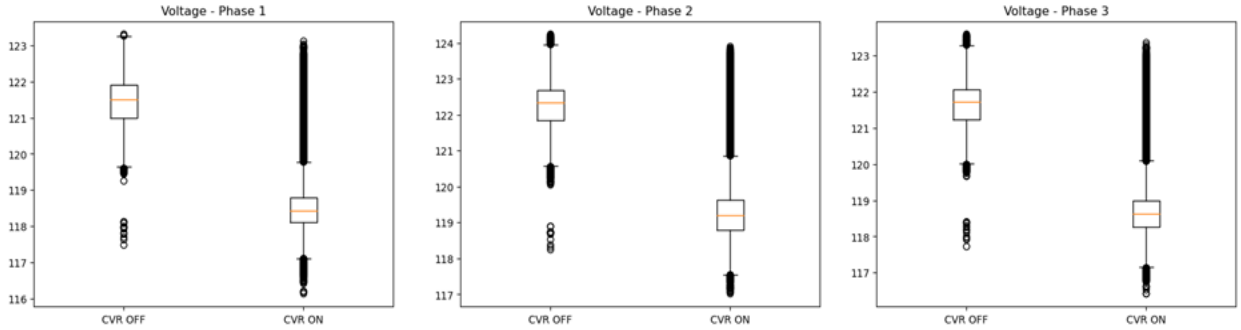

Figure 4.1a.4. Impact of advanced CVR on voltage statistics at the VR secondary side.

Under this award, HNEI's Grid***START*** collaborated closely with the USMC Camp Butler team to diagnose issues related to the lack of reactive power (var) dispatch from the var sources. Although connectivity between the VVC controller and the inverter plants was established, power requests were not being transmitted. Due to the islanded nature of the hardware, support from the Camp Butler team was essential for onsite troubleshooting. To reduce the burden on the Camp Butler personnel and to facilitate a thorough diagnosis, we replicated the field system in their APSL using the same inverter model as installed at TH-415, along with an identical VVC controller and software. This setup allowed the team to recreate and analyze the communication issue observed in Okinawa. The troubleshooting process required an extensive code review to analyze in depth the software routines and the various communication protocols involved.

HNEI was ultimately able to replicate issues in the APSL, identifying the root cause of the communication issues, and implement a solution that enabled the inverter and controller to correctly receive and execute var command set points from the VVC controller. The solution developed in the APSL was then remotely implemented in the field at TH-415, in collaboration with the USMC Camp Butler team. As a result, the advanced CVR device, comprising the VVC controller and inverters, is now operational and executing its control algorithm to reduce voltage drop across the TH-415 transformer, utilizing an on/off schedule to assess controller effectiveness. The CVR-controlled VR remains in service, operating under one-day-on, one-day-off cycles as part of ongoing CVR algorithm implementation. The performance data collected from these field operations provides a robust dataset for validating the initial overall CVR factor and for developing specific CVR factors for different load types across the seven transformers.

Following the resolution of communication issues between the VVC controller and power inverters at TH-415, additional field tests were scheduled to further optimize the VVC controller's performance and to quantify its contribution to overall CVR-energy savings. However, the field testing and evaluation activities were suspended in May 2025 due to the stop-work order.

4.1b Holistic Optimization of Microgrids: Enhanced Resiliency Schemes

The traditional power grid—largely dependent on fossil fuels—struggles with flexibility and resilience, particularly in remote or infrastructure-sensitive regions like Hawai‘i. Microgrids, especially those capable of operating in both grid-connected and islanded modes, offer a promising alternative by leveraging distributed energy resources (DERs) such as photovoltaic (PV) systems, battery energy storage systems (BESS), and hydrogen technologies. To address the growing need for resilient microgrids in grid-challenged environments, HNEI developed a holistic optimization framework to enable microgrid planning and design with a focus on resiliency, cost-effectiveness and integration of DERs under APRISES21 funding. This work fills critical gaps in existing modeling tools and was motivated by rising energy demands and the need for reliable, localized power solutions.

The Natural Energy Laboratory of Hawai‘i Authority (NELHA) in Kailua-Kona on the island of Hawai‘i (Figure 4.1b.1) served as the case study site for this project due to its existing DER infrastructure, the availability of high-resolution load and solar data, and its unique integration of a hydrogen electrolyzer for refueling hydrogen buses. This provided a real-world context to evaluate the developed solution under various operational scenarios. The final model delivered actionable recommendations for microgrid sizing and demonstrated the viability of green hydrogen, which is hydrogen produced through the electrolysis of water using electricity generated from alternative energy resources, for microgrid integration to enhance system resilience and reduce energy costs at NELHA.

Figure 4.1b.1. Aerial view of the NELHA case study site.

The core objective of this project was to develop a robust, adaptable optimization framework capable of recommending cost-effective, technically viable, and resilient microgrid configurations. To achieve this, a hybrid model combining mixed-integer linear programming (MILP) and particle

swarm optimization (PSO) was developed and applied to a real-world test case at NELHA. Figure 4.1b.2 presents the flowchart of the hybrid MILP-PSO approach used in this study. The model simulates both financial and technical performance metrics while allowing customization of DER configurations, hydrogen infrastructure, load prioritization, and time-of-use (TOU) pricing schemes.

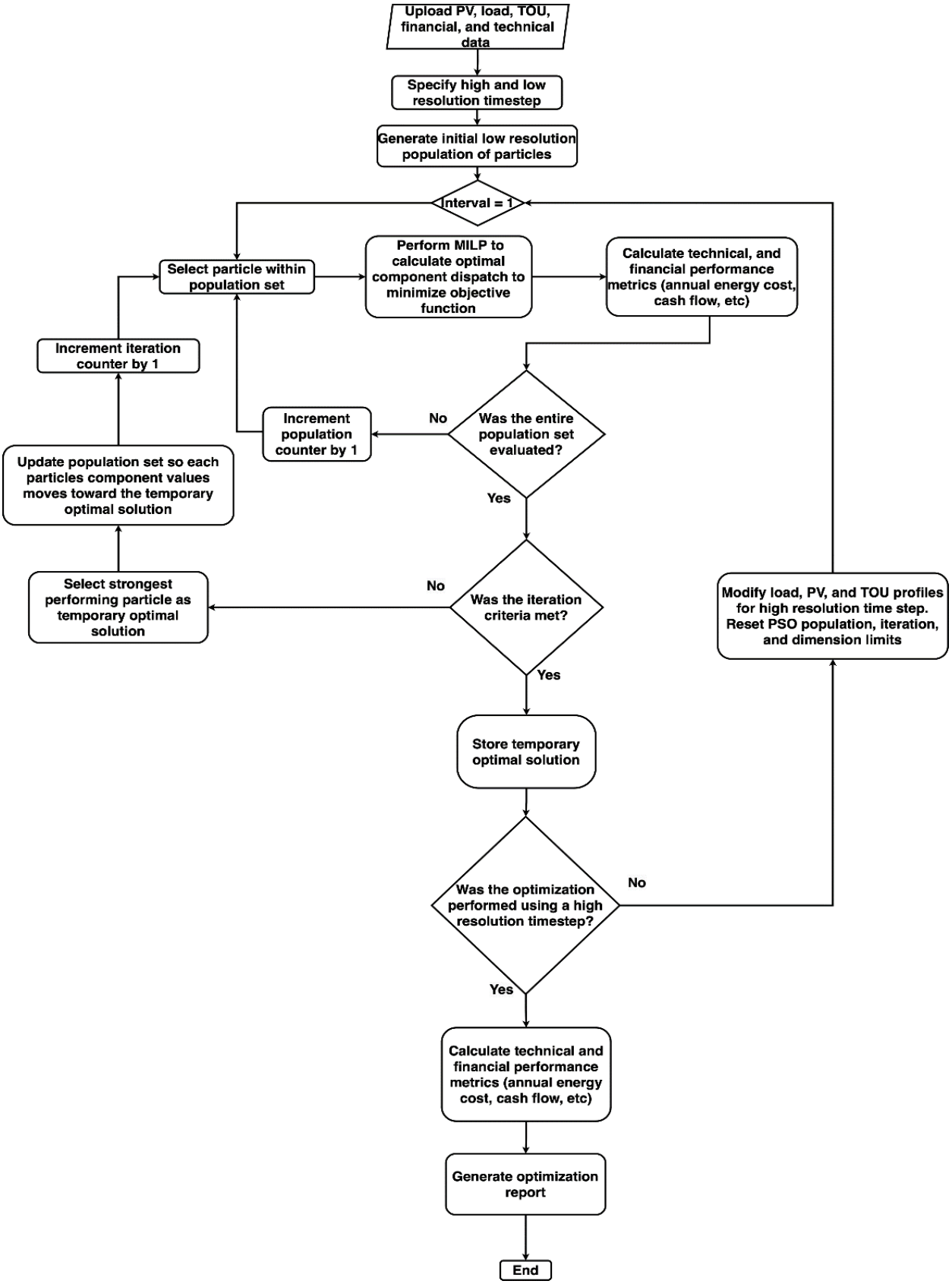

Figure 4.1b.2. Hybrid MILP-PSO flowchart.

The optimization model was designed to simulate and evaluate a complete 25-year system lifespan across five distinct operational scenarios:

1. Grid-connected operation without outages;
2. One-day resiliency with 100% load support;
3. Three-day resiliency with 100% load support;
4. One-day resiliency with 50% critical load support; and
5. Three-day resiliency with 50% critical load support.

These scenarios allowed both steady-state operations and emergency response capacities for the NELHA microgrid to be captured. For each scenario, the optimization framework evaluated the optimal sizing and integration of the following DERs: 1) PV; 2) BESS; 3) proton exchange membrane (PEM)-type hydrogen electrolyzer (existing at NELHA); 4) hydrogen gas storage tank; 5) stationary hydrogen fuel cell; and 6) diesel backup generator(s).

To simulate realistic operating conditions, the model utilized one year of actual load and solar irradiance data from NELHA, including time-series values for gross demand and PV generation. Utility pricing was modeled using Hawaiian Electric Company's (HECO) Schedule TOU J rates, allowing the framework to dynamically account for energy purchase costs, demand charges, and energy arbitrage opportunities. A key innovation in the modeling approach was the incorporation of NELHA's actual power-to-hydrogen efficiency curve, which enabled a more accurate representation of electrolyzer performance. Unlike conventional models that assume linear hydrogen production, this framework supported nuanced control by initiating hydrogen generation only above minimum operational thresholds, thus enhancing overall system realism.

The PSO algorithm was employed to optimize the sizing of key DERs including PV, BESS, the hydrogen storage tank, and the diesel generator, while the MILP component handled operational dispatch decisions. The objective function aimed to maximize the system's net present value (NPV), subject to all energy balance and resilience constraints. The proposed hybrid optimization framework generated feasible and cost-effective microgrid configurations tailored to both normal operations and resiliency scenarios. Across all scenarios, the model consistently demonstrated its capability to identify system designs that minimize lifecycle costs while maintaining operational reliability.

A consistent trend observed across all scenarios was the critical role of DER flexibility. The model dynamically allocated DER capacity based on energy demand profiles, outage durations, and financial constraints. For instance, under grid-connected conditions, combinations of PV systems and BESS alone were sufficient to meet demand in a cost-effective manner. To quantify energy costs and DER contributions, Tables 4.1b.1 and 4.1b.2 summarize the annual energy charges and distribution for that base scenario. As shown in Table 4.1b.2, PV accounted for the largest share of energy supply (42.7%), followed by BESS (10.1%), highlighting a strong reliance on DERs

during normal operations. However, when resiliency constraints were introduced, especially for multi-day outages, the optimization model favored more diversified energy portfolios that incorporated hydrogen storage and stationary fuel cells. These additions improved system autonomy and resilience while avoiding the need for oversized battery capacity.

Table 4.1b.1. Scenario 1: Annual Energy Charges.

Energy Category	Consumption [kWh]	Rate [$/kWh]	Energy Charge [$]
Overnight	621,627	0.432426	268,808
Daytime	16,015	0.216213	3,462
Evening-Peak	12,201	0.648639	7,914
Annual Energy Charge	649,843	Variable	280,184
Reference Energy Charge	1,531,863	Variable	598,259
Annual Energy Savings	882,020	Variable	318,074

Table 4.1b.2. Scenario 1: Annual Energy Distribution.

Energy Category	Consumption [kWh]	Percentage [%]
PV	654,566	42.7
Battery	154,299	10.1
Fuel Cell	73,153	4.8
Generator	0	0
Utility Grid	649,844	42.2

A key advancement in this work was the realistic modeling and integration of hydrogen infrastructure. The model demonstrated the technical viability of hydrogen-based backup systems and quantified their economic impact within the broader DER portfolio. The hydrogen system, though relatively costlier on a per-kW basis than PV or BESS, became economically justifiable in scenarios with strict uptime requirements. By using NELHA's actual electrolyzer efficiency data, the model accurately captured the trade-offs between power input, hydrogen output, and storage cost. Figure 4.1b.3 illustrates the hourly dispatch of DER components during a three-day outage, highlighting the interplay of solar, BESS, and hydrogen fuel cell.

The financial performance of the optimized systems further validated the model's effectiveness. All configurations showed positive NPVs over a 25-year period, and internal rates of return (IRR) were generally in the range of 8-13%, depending on the level of resiliency required. Discounted payback periods ranged from 6 to 15 years. Figure 4.1b.4 indicates that even microgrids incorporating advanced hydrogen technology can achieve financial feasibility under well-planned configurations and operational strategies.

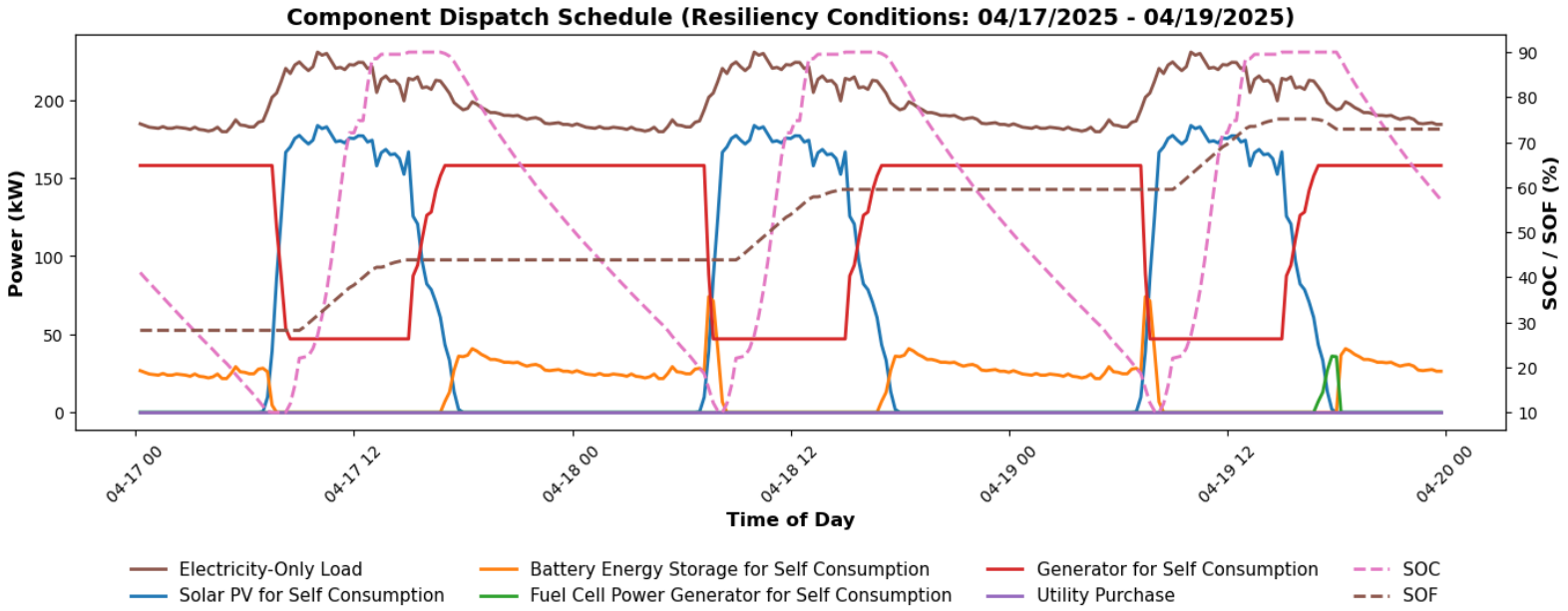

Figure 4.1b.3. Scenario 3: Resiliency conditions line dispatch schedule for April 17-19, 2025.

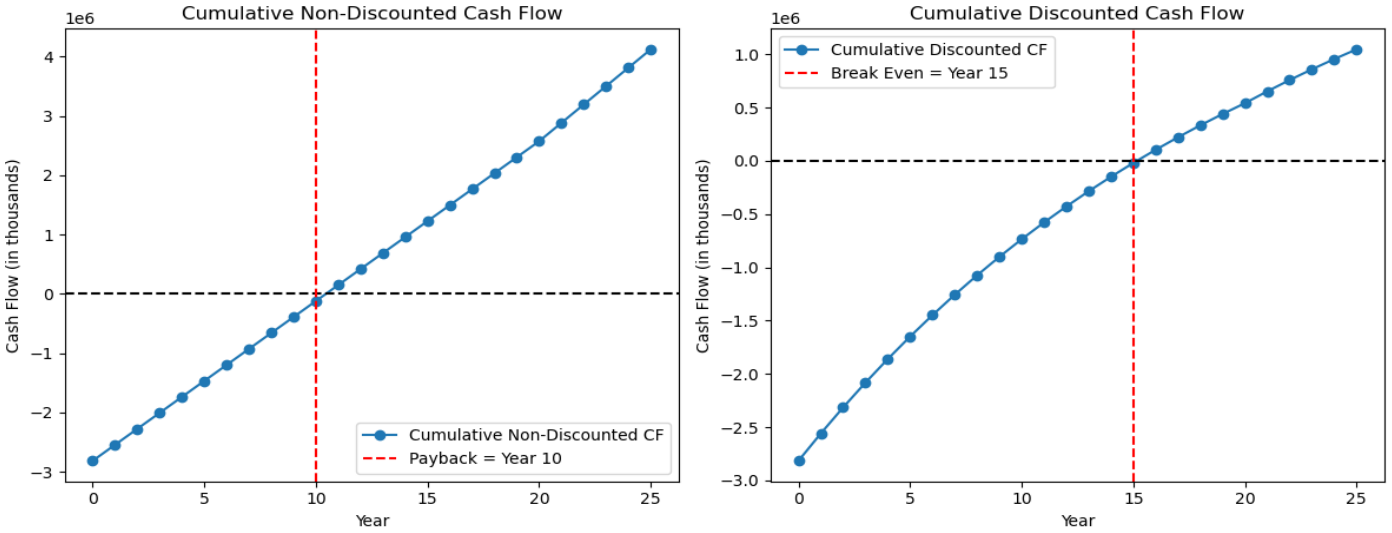

Figure 4.1b.4. Scenario 4: Non-discounted and discounted payback and break-even charts.

The model also revealed that operating under partial critical load conditions, such as supporting only essential loads like aquaculture pumps on the NELHA campus, provided an effective trade-off between resilience and cost. In these scenarios, system sizing and capital expenditures were significantly reduced while still maintaining critical functionality during outages.

Overall, this project successfully developed and demonstrated a hybrid optimization framework for designing resilient and cost-effective microgrids, using NELHA as a real-world case study. By integrating MILP with PSO, the model identified optimal configurations of PV systems, BESS, and hydrogen infrastructure for both normal and emergency operating conditions. The results of the simulation were validated by comparing them with NELHA's actual electric bill costs from HECO. Additionally, the framework was assessed using real-world load and solar irradiance from NELHA and Hawai'i, and was evaluated across multiple outage and resiliency scenarios. Results confirmed that a flexible, data-driven approach can generate economically viable DER portfolios while enhancing operational autonomy and grid resilience.

This work addressed key limitations in existing modeling tools by incorporating realistic hydrogen production curves and TOU rate structures. Furthermore, it demonstrated the practical feasibility of integrating green hydrogen technologies into microgrid systems, thereby advancing the state of the art in microgrid design and operation.

In addition to its technical contributions, this project provided valuable professional development opportunities for the graduate student who led the research. Through close mentorship and hands-on experience in optimization modeling, energy systems analysis and technical writing, the student gained expertise in advanced simulation techniques, alternative energy integration and applied research methodologies. The academic outputs from this project include a successfully defended master's thesis, a published peer-reviewed journal article and an additional manuscript currently in preparation for submission. These outcomes lay a foundation for future academic dissemination on hybrid optimization techniques and the integration of hydrogen technologies to enhance microgrid resilience. With the successful completion of modeling, validation, and scenario testing, and with results disseminated, this project is now concluded.

More detail on this work can be found in the *Energies* publication and thesis listed below. A citation and link to the additional manuscript will be accessible at https://www.hnei.hawaii.edu/publications/project-reports/aprises-21/ when available.

Publications and Presentations

Peer-Reviewed Publications

1. Kerkau, S., Sepasi, S., Howlader, H. O., & Roose, L. (2025). Day-ahead net load forecasting for renewable integrated buildings using XGBoost. *Energies*, *18*(6), 1518. https://doi.org/10.3390/en18061518

Student Thesis

1. Kerkau, S. M. (2025). *Resiliency-centric optimization for microgrid sizing: A holistic approach with renewable and hydrogen energy infrastructure*. Master's Thesis, Department of Electrical Engineering, University of Hawai'i at Mānoa, Honolulu, HI.

4.1c Coconut Island DC Microgrid Project

Under previous funding, HNEI's installed and commissioned a DC-based microgrid testbed on Coconut Island (Moku O Lo'e), a 28-acre (113,000 m²) island in Kāne'ohe Bay, O'ahu. The site, home to the Hawai'i Institute of Marine Biology (HIMB), serves an ideal location for testing energy security and grid-edge technologies due to its physical isolation and critical power needs. The island operates as an inherent microgrid through an undersea electrical connection. Its tropical marine environment, characterized by strong coastal winds and heavy salt spray, provides conditions similar to Navy coastal installations, making it suitable for testing new materials and technologies.

The project pursues a dual mission: providing locally sourced and secure power on the island via a DC microgrid testbed system and equipping the island with transportation options that utilize power sourced from a DC microgrid. To achieve this, it focuses on six key goals:

1. Demonstrate the capabilities of cutting-edge energy technologies within the microgrid;
2. Improve the reliability of electricity for the crucial infrastructure, reducing the island's reliance on the aging undersea electrical connection to the local utility;
3. Establish a research platform to evaluate DC microgrid resources and components, such as energy storage, supporting grid technology, and DC-powered equipment, all in a coastal tropical environment;
4. Develop and test energy security and operational algorithms that optimize the use of the microgrid's energy resources and the trade-offs between energy cost savings and resiliency;
5. Increase the island's energy security by maximizing the utilization of on-island energy resources; and
6. Offer electric-powered land and sea-based transportation options for HIMB that utilize on-island energy resources.

The project integrates a DC power distribution system into two existing buildings on the island, the Marine Mammal Research Project (MMRP) building and the adjacent Boat House, shown in Figure 4.1c.1.

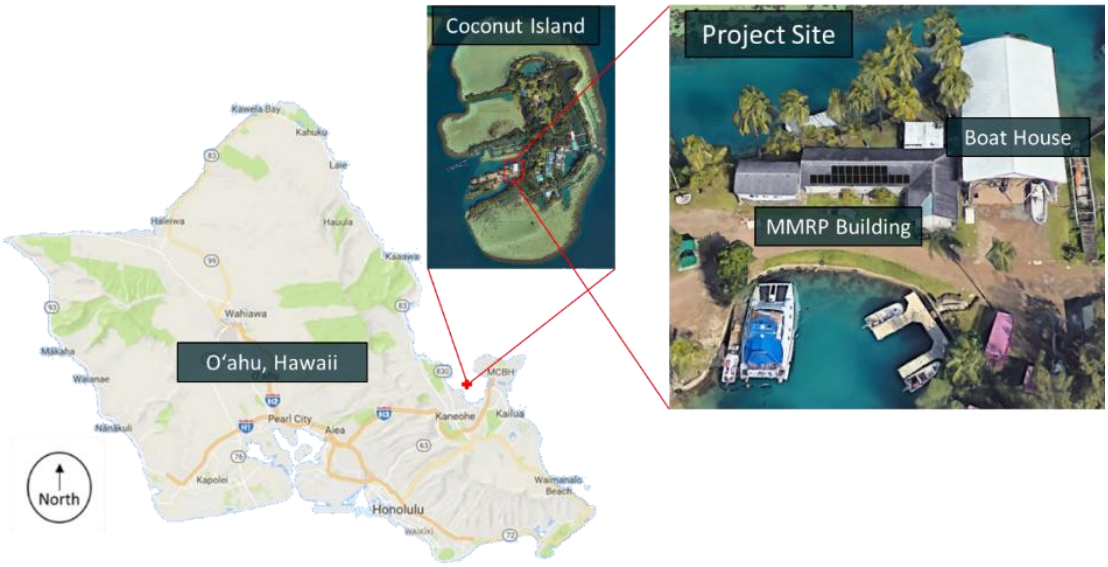

Figure 4.1c.1. Location of Coconut Island and the DC microgrid project site.

Prior APRISES funding supported the extensive development and deployment of the Coconut Island DC microgrid project through several key phases:

- *Initial Planning and Design*: The project began with detailed planning, permitting, and baseline energy data collection. A conceptual DC microgrid design was developed, informed by technoeconomic simulations to determine appropriate sizing for the MMRP rooftop photovoltaic (PV) system and stationary battery energy storage system (BESS) to serve selected loads within the MMRP building and Boat House. Detailed electrical design drawings were prepared by a licensed electrical engineer for the installation of the DC microgrid components.
- *Electric Boat (E-boat) Implementation*: PV panels were installed on the E-boat rooftop to support powertrain battery charging and auxiliary equipment operation. This phase included rigorous testing and commissioning, culminating in operational sea trials to verify functionality.
- *Infrastructure Development*: Major infrastructure procurement and installation activities included: 6.2 kW DC rooftop PV system on the MMRP building; 8 kW/8 kWh stationary BESS; AC/DC powered air conditioning unit; AC/DC LED lighting system; DC-to-AC inverter for critical plug loads; multi-point metering system for power flow monitoring; OPTO 22 Edge industrial controller (DC microgrid controller) and associated components; control system contactors and switch boxes; Schneider XW-Pro Inverter (capable of both DC-to-AC and AC-to-DC conversion, primarily used as an AC-to-DC inverter) with two maximum power point tracking (MPPT) charge controllers; and DC distribution system wiring.
- *Swappable Battery Charging Station and Associated E-car and E-boat*: In collaboration with the Okinawa Institute of Science and Technology (OIST) and PUES Corporation in

Japan, HNEI specified, designed, and procured a prototype E-car and E-boat, along with a swappable battery system and charging station powered by the DC microgrid. The swappable battery units and charging station were installed, commissioned, and tested with the E-car and E-boat. The project faced technical challenges, including conflicts between the battery management system (BMS) protection and the charging station, as well as ineffective charge balancing between battery cells within each battery unit. HNEI provided troubleshooting and maintenance to keep the battery units operational. Due to end-of-life issues and increasing failure rates, the swappable battery units and charging station were decommissioned during the APRISES19 funding period, and fixed placement battery systems were subsequently installed in both the E-boat and E-car for reliable operation.

- *System Integration and Control*: The team implemented advanced control systems, including: custom control programming using Node-RED and JavaScript; enhanced monitoring through high-voltage sensors; and comprehensive power flow monitoring capabilities.
- *DC Microgrid System Upgrades and Enhancements*: A new OPTO22 Controller was installed and commissioned as the core component of the DC microgrid, enabling robust real-time data processing and advanced automation for both AC and DC operating modes. The DC microgrid controller was enhanced with improved programming logic, a comprehensive control scheduler, and a user-friendly Node-RED interface for intuitive schedule management and seamless mode transitions (AC, DC, or hybrid). A real-time monitoring dashboard was developed, featuring Groov View visualizations, an interactive user interface, and backend integration of Node-RED and JavaScript for responsive system monitoring, remote access, and proactive issue alerting. PV system data download capabilities were enabled for historical data analysis, performance evaluation, and operational optimization.
- *E-boat Battery and PV System Upgrades*: The E-boat's batteries were upgraded from the 11.2 kWh swappable units to more robust 18.2 kWh fixed placement batteries, improving reliability and enabling future vehicle-to-grid (V2G) integration with the DC microgrid. Two separate PV arrays were consolidated into a single streamlined system, doubling the PV capacity and simplifying the design for extended operational periods and higher energy demands. Initial laboratory testing of V2G functionality demonstrated the E-boat's potential for bidirectional energy flow and enhanced grid integration.
- *Efficiency Evaluation*: After commissioning, Grid***START*** evaluated the DC microgrid's operational efficiency by periodically switching the air conditioning and LED lighting systems between DC and AC modes using the OPTO22 controller to directly compare energy usage. Plug loads and swappable battery system were excluded, as plug loads used only AC and the battery system was decommissioned. Results showed the air conditioner achieved an average efficiency gain of about 3.3% in DC mode, while LED lighting power consumption was approximately 5% lower in DC mode, highlighting further energy savings potential with optimized DC operation.

Over previous APRISES funding, the E-boat has undergone substantial development to enhance operational reliability, safety, and its potential for research in marine electrification and grid integration. Early efforts focused on the integration of PV panels on the E-boat's rooftop to help charge the propulsion batteries and auxiliary equipment. These efforts included rigorous testing, commissioning, and successful sea trials to validate system performance and functionality.

Initial development also included a swappable battery and charging system, designed in collaboration with the OIST and PUES Corporation. The system, powered by the DC microgrid, provided energy through battery units that supported both an E-boat and E-car. Following installation, the system underwent commissioning and testing, but reliability challenges emerged over time, most notably, incompatibility between the BMS and the charging station, as well as ineffective charge balancing within each battery unit. Despite HNEI's ongoing troubleshooting efforts, the system eventually reached end of life and was decommissioned during the APRISES19 period. To ensure consistent performance, both vehicles were upgraded with fixed-placement battery systems.

With support from APRISES21 funding, upgrades to the E-boat's energy systems included replacing the original 11.2 kWh swappable batteries with robust fixed 18.2 kWh battery packs, enhancing operational safety, reliability and enabling future V2G functionality. The physical system enhancements included the integration of the new stationary battery system, along with a battery converter, updated charge controller, and upgraded switching mechanisms and safety fuses. Rooftop PV arrays were also consolidated and expanded, doubling capacity, and paired with MPPT charge controllers for optimized solar energy capture and simplified power architecture to support extended operations. More specifically, to simplify system design and improve efficiency, the separate 12 V solar system was removed in favor of a fully integrated 48 V solar MPPT system. This unified solar configuration now delivers up to 1,980 W, enough to supply nearly 8 kWh in four hours of peak sunlight. This approach not only boosts recharging efficiency, but also simplifies maintenance and operation. These enhancements ensured that the E-boat could better meet increasing energy demands and laid the groundwork for advanced bidirectional energy integration with the DC microgrid infrastructure. Initial lab tests confirmed the E-boat's V2G capability and bidirectional energy flow potential.

The team also addressed critical design issues to enhance electrical and operational safety. For instance, the original placement of the charge controller beneath a seating area posed some risk with limited emergency access. In the revised design, the charge controller was repositioned beneath the aluminum boat roof and enclosed in a weather-resistant, National Electrical Manufacturers Association-rated (NEMA)-rated aluminum enclosure (see Figure 4.1c.2a). This strategic placement uses the aluminum structure as a passive heat sink, increasing thermal management and overall safety. An emergency disconnect switch was also installed adjacent to the main circuit breaker, enhancing rapid shutdown and serviceability (see Figure 4.1c.2b).

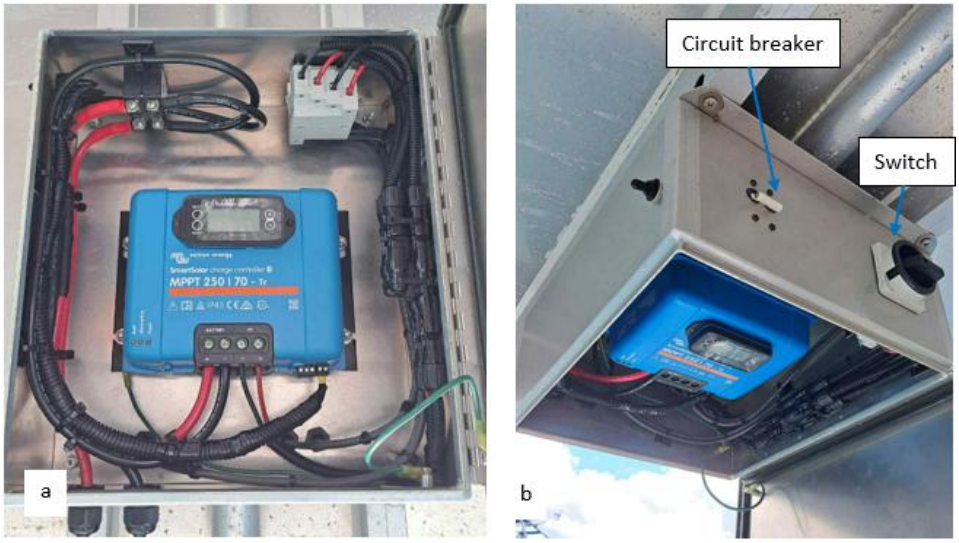

Figure 4.1c.2. a) MPPT PV charge controller and b) emergency shutoff/switch (NEMA box).

In terms of propulsion architecture, the previous dual-power (12 V and 48 V) system was eliminated due to reliability concerns where a 12 V system failure could disable the vessel, even with fully charged propulsion batteries. The new system uses four 48 V battery units operating in parallel, each with its own BMS. This redundant and fault-tolerant design allows continued propulsion at full capacity with three batteries, reduced capacity with two, and navigational maneuvering with even one unit. The critical propulsion control system now operates independently of the 12 V system, which has been retained only for non-essential loads and remote relay activation. Manual relay control remains available in the event of 12 V system failure, ensuring that essential functions can still be operated. This aviation-inspired approach prioritizes redundancy, resilience and fail-soft behavior, enabling safe navigation under a variety of failure scenarios (Figure 4.1c.3).

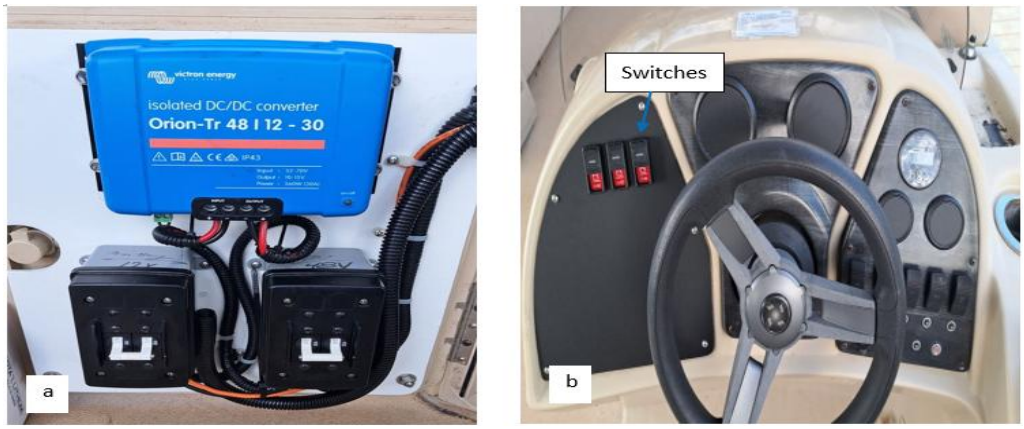

Figure 4.1c.3. a) Auxiliary 12V power converter and b) battery connect/disconnect switches.

All critical hardware components were thoroughly tested before and after installation to verify proper functionality. Figure 4.1c.4 shows the testing of the PV and battery connections, as well

as the available configuration options. These comprehensive enhancements not only strengthen the E-boat's capacity for reliable operation but also position it as a research platform for marine energy integration and resilience.

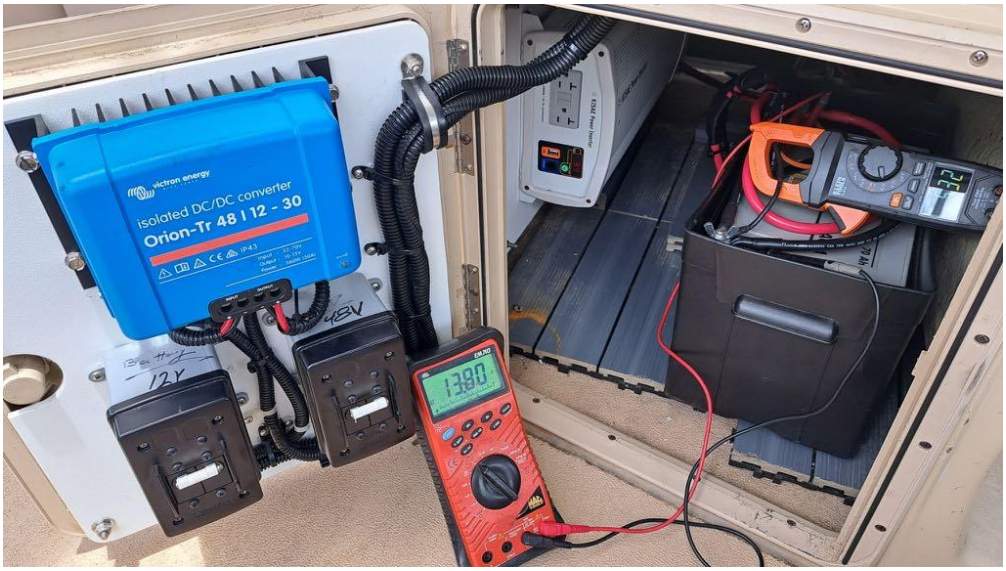

Figure 4.1c.4. Testing of the auxiliary 12V power converter.

Building on these achievements, the team identified several key focus areas for future research. Early lab tests of V2G demonstrated the E-boat's ability to manage DC bidirectional energy exchange, drawing power from the DC microgrid and supplying energy back as needed. With anticipated APRISES funding, the team aimed to integrate a dedicated controller and shore power connection, fully enabling the E-boat as a bidirectional power resource for the DC microgrid. This would leverage the vessel's mooring time and battery capacity for grid support, increasing the round-trip efficiency (RTE) of battery packs, which naturally degrade over time regardless of usage cycles.

The project's real-world prototype suggests that cost parity with internal combustion vessels is within reach, while also highlighting opportunities for advancing marine-specific ultra-low noise and low-emission technologies. Replacing traditional land-based solar panels with purpose-built marine bi-facial panels, which exploit the water's reflective properties, could potentially raise output to 3 kW without increasing the physical footprint. These upgrades represent a pivotal step in enhancing the microgrid's technical capabilities and positioning the system as a leading research platform for electric maritime transportation. Enabling V2G operation would yield critical data on electric propulsion in marine environments, offering globally relevant insights for coastal and island transport systems.

To our knowledge, this is the first 24-foot electric pontoon platform specifically designed for near-shore research and harbor support. It fills a critical gap in the market for small, ultra-quiet, exhaust-free vessels capable of handling daily logistical, monitoring, and educational tasks. This pilot

project offers a replicable, scalable model for institutions seeking to align operational practices with energy goals, demonstrating that electrified marine technology can be both practical and cost competitive.

Unfortunately, the sudden and unforeseen termination of APRISES funding has halted this forward-looking research. The funding served as a foundational pillar for transformative work at the intersection of energy, marine environments and technology. Its loss abruptly halted the ability to build upon the significant progress made, curtailing opportunities for further transformative impacts, and is a setback not only to the project team, but also the broader academic, policy, and community stakeholders who stood to benefit from advances in secure and effective energy infrastructure and transportation.

4.2 Resilient Grid Systems

Over the past decade, Hawai‘i has experienced rapid growth in solar energy driven by high oil prices, decreasing costs of solar technologies, and a commitment to reducing the use of fossil fuels. The first phase of large-scale solar integration began with the adoption of distributed rooftop systems—encouraged by net energy metering policies that allowed homeowners to offset electricity costs and receive credit for surplus energy produced. This program led to a significant increase in rooftop solar across the islands, as early adopters installed systems that contributed to the state’s renewable energy goals.

The second phase of solar expansion, currently underway, is dominated by the development of larger-scale utility solar projects, particularly on O‘ahu. Between 2017 to 2020, O‘ahu added 175 MW of utility-scale solar without battery storage, addressing daytime energy needs and further reducing the reliance on oil-fired generation. However, by the time these projects came online, mid-day solar generation regularly exceeded half of total demand and there was limited ability to integrate additional solar without storage into the grid.

Beginning with a request by the utility for proposals for dispatchable renewable energy in 2019, a third phase involving hybrid solar and battery storage projects was initiated. These projects that generate electricity during the day can store a significant amount of the energy generated for use during the evening or early morning peak demand periods. Through recent and expected future competitive procurements, this new generation of hybrid projects are expected to significantly increase the renewable energy share on the grid. Relative to the size of the Hawai‘i grids, these hybrid solar and storage systems are being deployed at a scale not yet seen in other parts of the United States or globally.

In previous work, HNEI, in collaboration with Telos Energy under contract to HNEI, developed probabilistic analytic tools to assess the reliability or island grids with very high penetration of variable renewables (solar and wind) with and without large scale energy storage. This effort leveraged resources from the Energy Systems Development Special Fund (ESDSF) managed by HNEI (also known as "barrel tax") and supported the Memorandum of Agreement between the State of Hawai‘i and the ASN for Energy, Installations and Environment, and also the Memorandum of Agreement between the University of Hawai‘i (UH) and the Pacific Command.

This research included efforts to quantify the requirements for dispatchable firm capacity on O‘ahu and the other islands' grids as increasing amounts of variable renewable generation and battery storage are deployed. It was found that, even with the relatively consistent wind and solar resources such as found in Hawai‘i, firm capacity of up to 60% of the peak load was required even when the variable renewables provided up to 90% of the total energy. This analysis was applied to quantify the reliability of the O‘ahu grid, pending the retirement of O‘ahu's largest generator, the AES coal plant, in September 2022 and to assess the value of the 560 MWh Kapolei Energy Storage standalone battery to mitigate the loss of generation due to the coal plant's retirement. A user-friendly tool was developed to allow stakeholders to track schedule changes in replacement resources and the impact on system reliability.

Under this award, these tools were used to evaluate the firm power needs to maintain O‘ahu resource adequacy as HECO retires other units. Analysis of the O‘ahu grid strongly suggests that integrating large-scale solar paired with storage can allow Hawai‘i's grids to receive up to 70% or more of their energy needs from variable renewable generation while keeping solar curtailment—the excess energy production that cannot be delivered to the grid—relatively low. Figure 4.2.1 shows that a modest curtailment allowance of less than 2% would allow up to 70% of the island's electricity from variable renewables (solar plus storage).

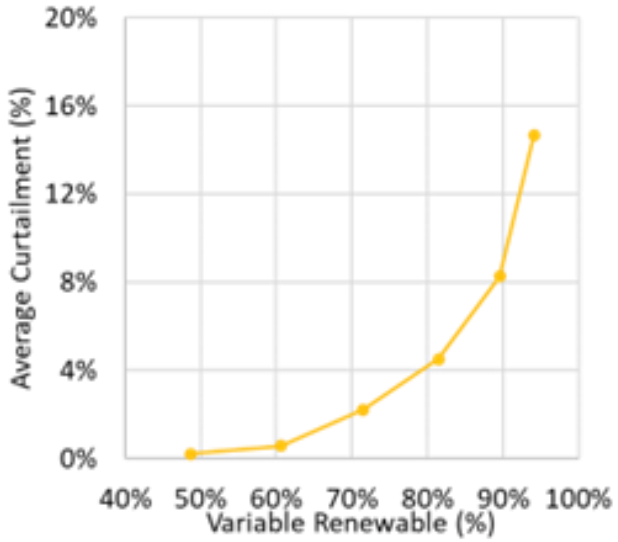

Figure 4.2.1. Solar curtailment at increasing shares of variable renewable energy.

Modeling also shows, that, even at the higher solar penetration levels (70% of energy), significant firm resources will be required to meet load when several consecutive days of low variable resource (wind, solar) are experienced. Figure 4.2.2 shows representative unit operation for one week of high solar resource and one of low solar resource, the latter requiring large amounts of dispatchable firm energy over several days.

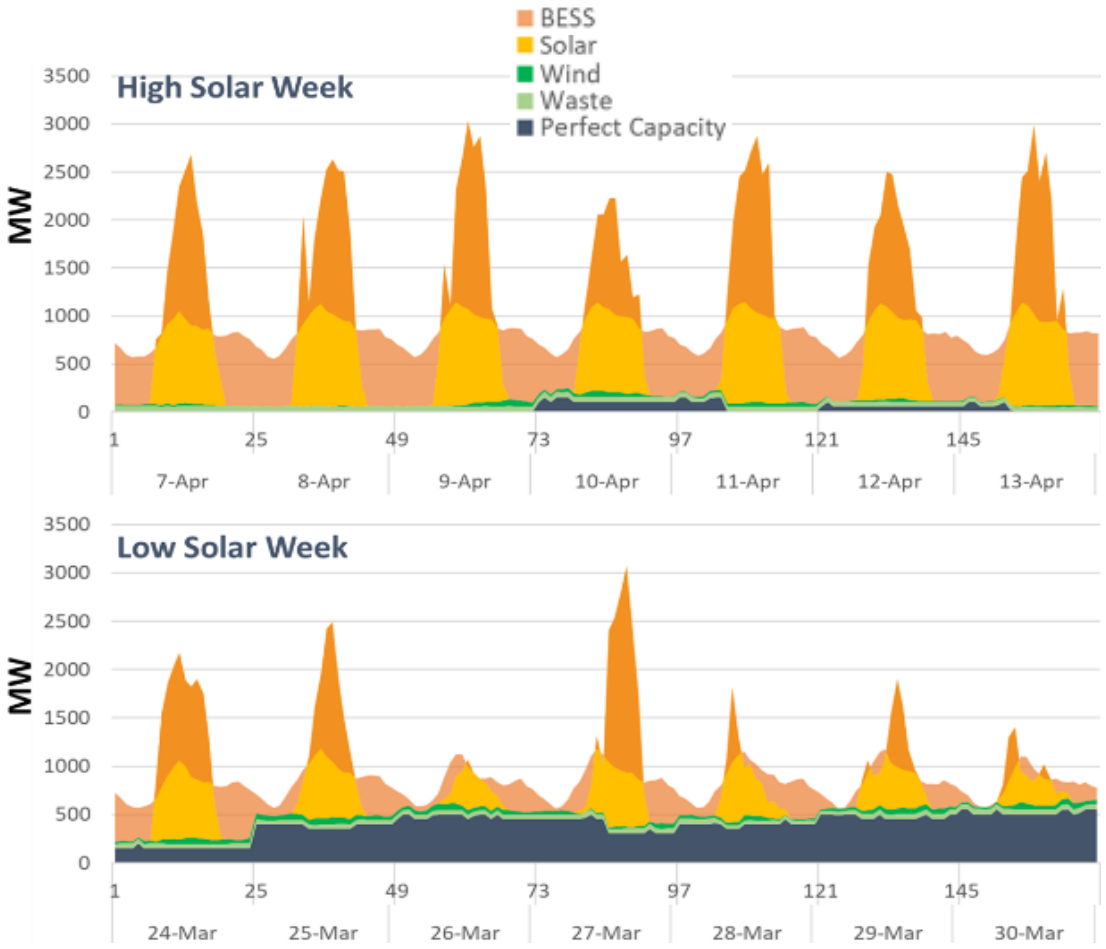

Figure 4.2.2. Representative high and low solar weeks and the need for firm renewables.

The utility's current plans call for retirement of the remaining Waiau steam plants between now and 2030. This includes the 100 MW from Waiau 3 and 4 retired in early 2025, 110 MW from Waiau 5 and 6 in 2027, and an additional 170 MW from Waiau 7 and 8 in 2029. Monte Carlo simulations for the different phases of retirement were conducted to assess the impact of retirement on O'ahu grid reliability and the potential benefits of proposed greenfield or repower projects.

Table 4.2.1 shows Loss-of-Load Expectation (LOLE), number of events per year during which a shortfall of generation might be expected. The column labeled 500 GWh corresponds to a solar penetration equivalent to the completion of all ongoing Stage 1 and Stage 2 RFP projects. As shown, at current solar penetration levels, the retirement of even Waiau 3 and 4 would result in a 6-fold increase in LOLE compared to today's O'ahu grid (approximately 0.22 LOLE). Not until

an additional 2500 GWh of solar was installed, corresponding to approximately a 70% penetration, could Waiau 7 and 8 be retired. This is not viable based on the HECO retirement timeline.

Table 4.2.1. Estimated Loss-of-Load Expectation for different solar penetration levels for different HECO retirement scenarios.

	Plant Name	Cumulative Retirement	500 GWh PV+BESS	1000 GWh PV+BESS	2000 GWh PV+BESS	3000 GWh PV+BESS
Incremental Retirement		0				
	AES	180				
	W3-4	274	**0.21**	**0.04**		
	W5-6	382	**0.95**	**0.24**	**0.01**	
	W7	466		**0.91**	**0.10**	**0.03**
	W8	551			**0.47**	**0.12**
	K1	635				**0.37**
	K2	720				
	K3	805				
	K4	889				
	K5	1024				
	K6	1159				

New projects submitted to the Hawai‘i Public Utilities Commission (HPUC) for approval include the 99MW Pu‘uloa project located at Joint Base Pearl Harbor Hickam (JBPHH). This project, being developed by Ameresco, Inc. in partnership with the U.S. Navy and Hawaiian Electric Company (HECO), will utilize 11 dual-fuel (diesel and biofuel) reciprocating generators. This project is intended to provide support to the O‘ahu grid and to provide backup power to JBPHH should an island wide black-out occur. The Pu‘uloa project will also include black start capability. The start-stop flexibility of this unit supports deployment of additional solar or other intermittent resources. This project was supported in part by the U.S. Department of Energy under its *Grid Resilience and Innovation Partnerships (GRIP) Program*, although that funding was recently identified for early termination.

HECO has also requested approval for the repower of the Waiau plant, proposing to replace their six aging oil-fired steam turbines with six modern, fuel-flexible simple-cycle combustion turbines intended for rapid dispatch. These fuel flexible units have a total capacity of 253 MW. Per HECO documents, these turbines would be able to operation on liquefied natural gas (LNG), petroleum, hydrogen, or biofuels. They also have black-start capability for resilience. The application for this repower was filed in March 2025 with a target commercial operation date of July 2033. Table 4.2.2 shows the estimated LOLE, assuming availability of the new Pu‘uloa plant and the completion of the repower for Waiau.

Table 4.2.2. Estimated Loss-of-Load Expectation for different solar penetration levels assuming full availability of Pu‘uloa and the Waiau repower.

	Plant Name	Cumulative Retirement	500 GWh PV+BESS	1000 GWh PV+BESS	2000 GWh PV+BESS	3000 GWh PV+BESS
Incremental Retirement		0				
	AES	180				
	W3-4	274				
	W5-6	382				
	W7	466				
	W8	551				
	K1	635				
	K2	720	0.10	0.01		
	K3	805	0.28	0.08		
	K4	889	1.41	0.31	0.04	
	K5	1024		1.94	0.29	0.08
	K6	1159			1.51	0.36

While retirement of Waiau without additional new generation was not feasible, completion of the Pu‘uloa facility and repower of Waiau would result in a significant increase in reliability compared to today’s grid. Even without additional solar (see 500 GWh column), LOLE would be below 0.10 days/year, consistent with mainland standards. Additional solar beyond the Stage 1 and Stage 2 projects would further increase reliability and proportionally decrease fuel use.

Given lead times for development of new generation, these decisions need to be considered in the near future. Potential solutions being considered by various stakeholders include continued use of oil, imported biofuels, or LNG. In prior work, HNEI also evaluated the energy and infrastructure needs to produce hydrogen using water electrolysis, store it, and convert it back to electricity to meet long-term firm power needs.

New generation, including the repower of Waiau is unlikely to be allowed to use the low sulfur fuel oil that is the current workhorse fuel for O‘ahu generation. Future fuels need to be carefully evaluated in regard to cost, availability, emissions, and impact on the operation schedules for the remaining older generation units. Additional options for the repower of the Waiau units will also be evaluated. We anticipate completing these fuel studies using funding from the Energy Systems Development Special Fund.

Publications with additional detail of the analysis are in process and will be accessible at https://www.hnei.hawaii.edu/publications/project-reports/aprises-21/ when available.

TASK 5: ADVANCED HEAT EXCHANGER DEVELOPMENT

Under multiple awards from ONR via the University of Hawai‘i, Makai Ocean Engineering has been developing Thin Foil Heat Exchangers (TFHX^{TM}) for use in seawater-refrigerant, air-water, and water-water applications. The work supported under APRISES21 was conducted between November 2024 and July 2025. In this period, Makai designed the next generation TFHX plate fabrication equipment; commissioned the new HX Testing Facility; performance tested two cassette-style 2-MWthermal TFHXs; developed concepts for large-scale seawater-water TFHXs; and prototyped new biofouling mitigation methods. Makai's efforts also included improving TFHX fabrication methods, continued characterization of TFHX thermal and structural/mechanical performance, and investigation of biofouling mitigation methods.

TFHX Design Development: Under this award, Makai finalized the pass-thru seawater air conditioning (TFAC) design and developed a cassette-style design for large-scale applications (>2 MWthermal) requiring large stacks of plates. The cassette design is expected to reduce the total unit cost by eliminating individual modules and improve performance by eliminating two 90° turns in the seawater path. Makai performed multiple measurements on 10 prototype-scale plates and found the shape and size of the internal channel was consistent and the measured deviations were unlikely to cause uneven heat transfer distribution between plates.

In cyclic pressure testing, Makai found an unsupported re-expansion step can lead to 3-8× increase in cycles prior to failure and shift failures from pattern welds to seal or transition welds. With an unsupported expansion, the internal channels become larger and more spherical which leads to more uniform distribution of stress. Lower ratios of alternating stress to support burst pressure, lead to longer cycles to failure.

Makai also delivered an air cooling unit (TFAC) to Blue Ocean Mariculture (BOM) and will be tracking performance once BOM installs it. Testing of the cassette-style design is planned in 2024 under separately funded work.

TFHX Fabrication: During this report period, Makai improved fabrication speed, implemented the post-expansion repair method, and improved the quality of the cut-edge. Plate fabrication time was improved from 16.7 min to 12.4 min with an overall success rate of 68%. During the first two days of the production run, plate success rate was 78.5%. Makai continues to investigate the inconsistency between the first two days' and last two days' success rates. The post- expansion repair method contributed ~20% of the successful plates.

Finally, Makai identified the quality of the cut-edge was sensitive to the distance between the surface and the laser. New fixturing commissioned in this period provided better control of the distance and improved the quality of the cut edge; however, some sections are still rough. Makai plans to incorporate z-stage motion on the laser to produce a consistently smooth cut edge.

TFHX Performance Testing: In this period, Makai fabricated four TFHXs for seawater-ammonia testing. Three of the four heat exchangers have been tested, each as an evaporator and a condenser. One heat exchanger remains to be tested.

Makai tested three ammonia-seawater (ocean thermal energy conversion, OTEC) four-port TFHXs. Performance data is fed into the OTEC Power Calculator to evaluate the different TFHX designs in the context of an OTEC power plant. The OTEC Power Calculator accounts for parasitic losses related to the total amount of seawater flow through the system, not just through the heat exchangers.

For a condenser, TFHX designs with larger plate spacings that optimize at higher volumetric flow rates are penalized because of the parasitic losses in the cold water pipe. For an evaporator, larger plate spacings that require higher volumetric flow rates are penalized because the intake screen must be larger to limit the approach velocity. Larger plate spacings also increase the overall OTEC system volume, which leads to larger (and more expensive) support structures. However, there is also the issue of biofouling mitigation to consider when selecting the evaporator design. Larger plate spacings may be easier to clean and ultimately lead to higher performance because the heat transfer surfaces won't be fouled.

TFHX designs tested in this period were compared to previous designs in the OTEC Power Calculator. The best designs were TFHX-FL1 and TFHX-FL4 for the evaporator and condenser, respectively. However, the optimized operating point was outside the tested range for TFHX-FL1 and, therefore, Makai has selected TFHX-FL12 as the new evaporator design. TFHX-FL12 is predicted to produce 3.5% less net power compared to TFHX-FL1, but the operating point was within the tested data range, providing more confidence in the prediction.

Biofouling: During this reporting period, Makai tested various methods of mechanical brushing and implemented a Velcro brushing method in an automated in situ cleaning prototype. Makai also started a baseline (no biofouling mitigation) test on a 3.17-mm spacing four-port TFHX unit for comparison. In both the brushed and baseline units, there was no change in pressure drop vs. flow after 30 days (as expected). Under future funding, testing will continue for at least 90 days. In previous tests, performance degradation was observed within 90 days. Makai also continues to investigate different types of brushes and passive mechanisms to remove biofouling.

Future, near-term efforts will include efforts to:

- Identify factors in fabrication environment and/or procedure that lead to inconsistencies in plate success rates;
- Improve cut edge quality;
- Continue SW-NH3 performance testing to identify optimal OTEC design; and
- Continue to develop, prototype and test in-situ biofouling control/mitigation systems.

More detail on Makai's research under this task can be found in their final report to HNEI, which is available at https://www.hnei.hawaii.edu/publications/project-reports/aprises-21/.